Suplemento de la Revista Mexicana de Física **1** (4) 32–53 SEPTEMBER-OCTOBER 2020

A zodiac of studies on complex systems*

A. Robledo[a] and L. J. Camacho-Vidales[b]

[a]*Instituto de Física y Centro de Ciencias de la Complejidad, Universidad Nacional Autónoma de México.*
[b]*División de Ciencias e Ingenierías, Universidad de Guanajuato.*
**Based on one of twelve zodiac lists for the same twelve sets of studies*

Received 26 May 2020; accepted 17 June 2020

We offer a brief description of a set of interrelated research lines on the physics of complex systems developed under a unifying methodology grown out from nonlinear dynamics of low dimensionality. The research lines were, and are, developed over a two-decade period (tacitly or not) under a simplifying assumption (and a posteriori corroboration) of a drastic reduction of degrees of freedom. The studies are conveniently grouped into twelve units, and these in turn into four groups, as in a zodiac. The studies in the first group, named Sensitivities, Glasses and Localizations, have in common a clear-cut original opening in the sense that, to our knowledge, the main tenet or result is not found elsewhere. Those in the second group, named Sums, Rankings and Fluctuations, have as a starting point previous stimulating studies or ideas that we followed up but then we converted into separate approaches. The subjects in the third group, named Networks, Measures and Games, involve preset work programs to be followed but ended up within unanticipated, perhaps deeper, grounds. The topics in the final fourth group, named Partitions, Diagonals and Windows, occurred, or are taking place, as specific technical goals that have become after belated realizations to be possible contributions towards the answer of fundamental quests. We discuss connections underlying different aspects of these investigations.

Keywords: Complex systems; nonlinear dynamics; low dimensional chaos; criticality; self-Organization.

PACS: 89.75.-k; 05.45.-a

1. Introduction

During the last twenty years we began, increased and consolidated a linked set of research lines dedicated to the investigation of complex systems. This set rests on independent, original and rigorous developments [1,2], which are integrated into a coherent structure for the understanding, and subsequent use, of the transitions to chaos in the so-called dissipative nonlinear systems of low dimensionality [3-5]. Two groups of properties have been obtained and further developed into effective research tools: the dynamics *inside* and the dynamics *towards* the attractors that represent the transitions to chaos. Based on this knowledge, research on core problems of complex systems has been carried out. In the physics of condensed matter we have obtained results in problems of difficult treatment: glassy dynamics, localization and critical fluctuations. In complex systems we have achieved central results for evolutionary dynamics, ranked data distributions (Zipf and Benford laws), and, recently, on the rationalization and (needed) statistical-mechanical justification of the phenomenon of self-organization.

The significance of the results obtained so far rests on the observation that our low dimensional model systems capture the main behaviors of high dimensional complex systems. An extreme reduction of their degrees of freedom has been fittingly implied in our analysis. A common factor in our closely related lines of research has been the use of the same properties of dissipative non-linear dynamical systems of low dimensionality [1,2], particularly those at the transitions that these systems show between regular or periodic, and irregular or chaotic behavior. Our interest has been oriented to the study of the known routes to chaos exhibited by these model systems. We have contributed with very specific descriptions but of unprecedented detail that had remained unexplored: the dynamical properties at the transitions to chaos together with those towards the attractors involved. These properties are anomalous, in that they differ profoundly from both periodic and chaotic dynamics.

A few introductory words about the starting point contributions of the twelve sets of studies we describe below are: *Sensitivities*. A central quantity in nonlinear dynamics, the sensitivity to initial conditions, was determined explicitly for the pitchfork and tangent bifurcations as well as for the period doubling and the golden ratio quasi-periodic transitions to chaos [6-12], all of which display anomalous properties while their Lyapunov exponent vanishes. *Glasses*. The bifurcation gap, that encloses and shrouds the period-doubling and chaotic-band-splitting accumulation points, induced by the addition of external noise was shown to appear as a crossover phenomenon along time evolution at the onset of chaos [13-16]. *Localizations*. A vital recursion relation for size growth of a basic wave scattering model was recognized as a nonlinear iteration map with a bifurcation diagram where tangent bifurcations separate periodic (insulating) and chaotic (conducting) attractors [17-20]. *Sums*. The distributions for sums of successive positions of trajectories, as in random walks, for families of chaotic attractors of the quadratic map were found to conform to a renormalization group scheme such that its trivial fixed-point matches the central limit theorem [21-25]. *Rankings*. The size-rank distribution of all kinds of numerical data, including Zipf law, were seen to be ob-

tainable from nonlinear maps close to a tangent bifurcation, such that data samples are reproduced by their trajectories [26-32]. *Fluctuations*. The joint use of density functional theory (for inhomogeneous systems) and the renormalization group fixed-point map (for the tangent bifurcation) delivered a space-time description for the dominant fluctuation at a critical point [33-35]. *Networks*. The transformation of iterated map trajectories into (Horizontal Visibility) graphs opened the possibility of reevaluating the link of the renormalization group technique with entropy optimization, and likewise the generalization of the Pesin theorem at the transitions to chaos [36-42]. *Measures*. The alternative description of nonlinear dynamics via probability densities of ensembles of trajectories instead of the trajectories themselves gave access to statistical-mechanical viewpoints of known behaviors [43]. *Games*. The initial consideration of the discrete-time version of the replicator equation of conventional games leads straightway to novel bifurcation diagrams and valuable coupled-map models [44-46]. *Partitions*. From the start, the property that summarized our calculations for the dynamics towards the periodic attractors of the quadratic map resembled in form that of a partition function. Continued work supported this interpretation and finally a model for self-organization materialized [47-54]. *Diagonals*. Originally, we represented the (master) trajectory at the period-doubling onset of chaos in logarithmic scales and this revealed an infinite family of straight lines, or interwoven power laws, that subsequently led to many fruitful interpretations and analytical statistical-mechanical results [7,9,14,11,21,30]. *Windows*. The control parameter gaps that interrupt the chaotic attractor intervals in the bifurcation diagram of the quadratic map contain infinite families of reproductions of the bifurcation diagram itself, the gaps display power-law spacing and widths [55,56]. These features are caricature building blocks for current modeling of nested complex systems.

More details about these sets of studies are given in the following sections while future directions are delineated in the concluding section. Additional related reading and commentaries can be found in [57-66]. The significance of the results obtained so far rests on the observation that our low dimensional model systems capture the main behaviors of high dimensional complex systems. A common factor in our closely related lines of research has been the use of home-produced properties of basic dissipative non-linear dynamical systems.

2. Original beginnings

We shall see now how a generalized Pesin identity (linking evolution of trajectories to entropy growth) offers an ideal biodiversity 'tree of life' model. This requires knowledge about the sensitivity to initial conditions at the multifractal period-doubling onset of chaos. Next, we see that the ideal glass concept exists and can be precisely represented by the attractor at the onset of chaos. This requires the knowledge that the noise-induced bifurcation gap is recapitulated at such, perturbed, onset of chaos. Lastly, we see how the localization transition between conducting and insulating states in a model array of wave scatterers is described by the transition out of chaos at the tangent bifurcation. This requires the knowledge that the model properties are rigorously analogous to those of an equivalent nonlinear map.

2.1. Sensitivities

At the transitions to chaos in one-dimensional nonlinear maps the (only) Lyapunov exponent vanishes. A classical example is the period-doubling accumulation point attractor (for short, Feigenbaum attractor) present an infinite number of times in the bifurcation diagram of quadratic maps. There, the sensitivity to initial conditions ξ_t behaves anomalously; it fluctu-

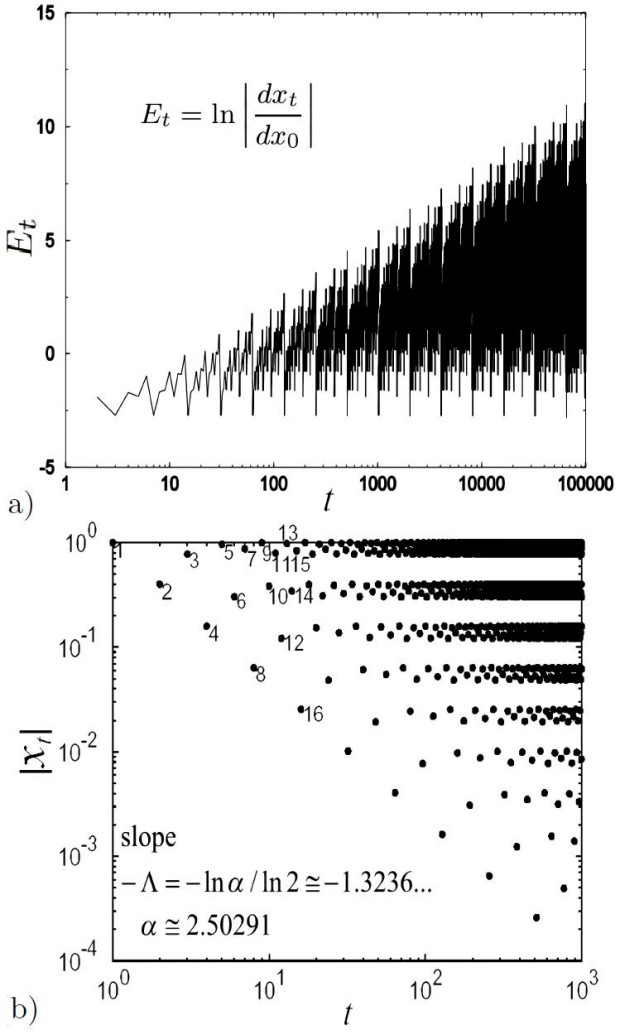

FIGURE 1. a) Sub-exponential growth and fluctuating amplitude of the expansion rate E_t shown for the first 10^5 iterations for the logistic map at the onset of chaos with initial condition $x_0 = 0$. b) Absolute values of positions in logarithmic scales of the first 1000 iterations for the trajectory as in a). The numbers correspond to iteration times. The power-law decay of the time sub-sequences described in the text can be clearly appreciated.

ates endlessly in iteration time t with increasing amplitude that grows sub exponentially. See the expansion rate $E_t \equiv \ln \xi_t$ in Fig. 1a). Insight on this behavior can be gained by examination of the trajectory on this attractor initiated at the extremum of the map. This is shown in Fig. 1b) in logarithmic scales, where the infinite number of parallel straight lines, mentioned before, can be observed running from the upper left corner to the lower right corner. With few exceptions, our calculations for quadratic maps have been performed with the logistic map version

$$f_\mu(x) = 1 - \mu x^2, -1 \leq x \leq 1, 0 \leq \mu \leq 2, \qquad (1)$$

for which locations of Feigenbaum points are denoted μ_∞. The trajectory initiated at $x_0 = 0$ when decomposed into position sub-sequences $x_t, t = (2k+1)2^n, n = 0, 1, 2, ...$, each for a fixed $k = 0, 1, 2, ...$, fall into straight lines we call diagonals. That is, the position sub-sequences obey power laws with the same exponent (slope in the figure) $m = -\ln \alpha / \ln 2 = -1.3236...$, where $\alpha \simeq 2.50290$ is the absolute value of Feigenbaum's universal constant [3]. The diagonals run from the most compact region at $x = 1$ to the most open region at $x = 0$ of the multifractal attractor.

Some elements of the sensitivity ξ_t can be determined from the diagonals. Nearby trajectories initiated at $x = 1$ will separate monotonously if observed at sub-sequence times as they approach $x = 0$, and vice versa when departure is reversed. The result in closed analytical form is [7,10]

$$\xi_\tau(x_0) = \exp_q[\lambda_q(x_0)\tau], \qquad (2)$$

where $\exp_q(x) \equiv [1 + (1-q)x]^{1/1-q}$ is the q-deformed exponential function. When $x_0 = x_{2k+1}$, times τ are of the form $\tau = (2k+1)2^n, n = 0, 1, 2, ...$, the q-deformation index is $q = 1 - \ln 2 / \ln \alpha$ and the q-generalized Lyapunov exponent is $\lambda_q = \ln \alpha / (2k+1) \ln 2$ [7]. On the other hand, when $x_0 = x_{2k}$, times τ are of the form $\tau = (2k)2^n, n = 0, 1, 2, ...$, the q-deformation index is $q = 1 + \ln 2 / 2 \ln \alpha$ and the q-generalized Lyapunov exponent is $\lambda_q = -2 \ln \alpha / (2k+1) \ln 2$ [10]. There are many other values for the q-generalized Lyapunov exponents as there are many other pairs of regions that trajectories can connect in the multifractal attractor. There is a spectrum for their values [10]. Notice that the sensitivity ξ_τ depends always on the initial condition x_0.

There is a remarkable property in the dynamics at the Feigenbaum attractor that leads to an identity between the q-generalized Lyapunov exponent λ_q and the rate of growth of the q-generalized entropy S_q. This is the counterpart of the Pesin identity that states the equality of the (positive) ordinary Lyapunov exponent λ_1 with the Sinai-Kolmogorov entropy K_1 for chaotic attractors [3-5]. This property is that a distribution, say uniform, of initial conditions within a small interval adjacent to, say $x = 1$, remains invariant for later iteration times, in this case chosen along the previously described diagonals (*i.e.* remains uniform at times of the form $t = 2^n, n = 1, 2, 3...$). The resulting q-generalized Pesin identity reads [9]

$$\lambda_q \equiv t^{-1} \ln_q \xi(t) = K_q \equiv t^{-1} S_q(t), \qquad (3)$$

where the q-logarithm $\ln_q(x) \equiv [x^{1-q} - 1]/(1-q)$ is the functional inverse of $\exp_q(x)$ and

$$S_q = \sum_i p_i \ln_q p_i^{-1}. \qquad (4)$$

As there is an infinite family, a spectrum, of q-generalized Lyapunov exponents λ_q, there is an infinite family of q-Pesin identities [10]. This property that indicates iteration time extensivity, remains, arguably, the most important exact result in q-statistics.

We advance here a preview of a first application of the q-Pesin identities that is taking shape only recently. This consists of an ideal model for diversity, intended for biological systems or other fields where diversity is of central position. Briefly, a backbone model for the evolution of a 'tree of life' and its limiting 'canopy', that could be used as a base to analyze, upon additions or modifications, more realistic circumstances. Recall first the familiar diversity index, Hill number, or effective number of species [67]

$${}^qD(R) = \left(\sum_{i=1}^{R} p_i^q \right)^{1/(1-q)}, \qquad (5)$$

where ${}^qD$ is the diversity index, R the richness (or total number of types or species in the data set), and the $p_i, i = 1, ..., R$, are the proportional abundances used in practice as nominal weights, but we consider normalization to identify them as probabilities. The parameter q defines a capacity of the diversity index to discriminate between rare and abundant species (similarly to its use in multifractals [3-5]). Use of Eqs. (3) and (4) in Eq. (5) gives

$$\lambda_q = \frac{1}{R} \ln_q({}^qD), \qquad (6)$$

or $\xi_t = {}^q D(R)$. The connection above requires $R = t = 2^n, n = 0, 1, 2, 3, ...$ and when $q = 1 - \ln 2 / \ln \alpha$ the entropy $S_q = \ln_q({}^qD)$ grows linearly with the richness R.

2.2. Glasses

It has been known for already a long time that the addition of noise to a quadratic map alters its bifurcation diagram introducing what is called a 'bifurcation gap' [3]. This gap consists of the removal of a strip of periodic and chaotic-band attractors with periods or number of bands larger than a threshold number $2^{N(\sigma)}$ where σ is the noise amplitude in the perturbed map

$$x_{t+1} = f_\mu(x_t) + \eta_t \sigma, \qquad (7)$$

and where η_t is a random, say Gaussian, variable. There is still a distinct transition to chaos at $\mu_\infty(\sigma)$ where the noise-perturbed ordinary Lyapunov exponent $\lambda_1(\sigma)$ changes

sign and the maximum value $N(\sigma)$ is attained. The noise-perturbed $\lambda_1(\sigma)$ obeys scaling properties around $\mu_\infty(\sigma)$, while $N(\sigma) \to \infty$ as $\sigma \to 0$ [3]. Dynamics at the Feigenbaum attractor is nonergodic if considered in terms of its noise-perturbed counterpart in the sense that the former is restricted into a multifractal space while the latter has access to a space-filling real number interval. The limit $\sigma \to 0$ can be referred to as an ergodic to non-ergodic transition.

It has also been some time since we pointed out an unusual connection between two seemingly different situations [13,14], one of them the bifurcation gap and the other glass formation. The first belongs to nonlinear dynamics and the second to condensed matter physics. It was shown that they share main defining properties: the gradual disappearance of diffusion, the scaling law known as aging, anomalous two-step relaxation, etc. [13-16]. Noise amplitude in one setting represents temperature difference ΔT to a vitreous state in the other. The two problems indicate loss of ergodicity as σ and ΔT vanish. And Eq. (7) can be seen to be a kind of discrete-time nonlinear Langevin equation. Nonetheless, in one case there is only functional composition while in the other there are molecular collisions.

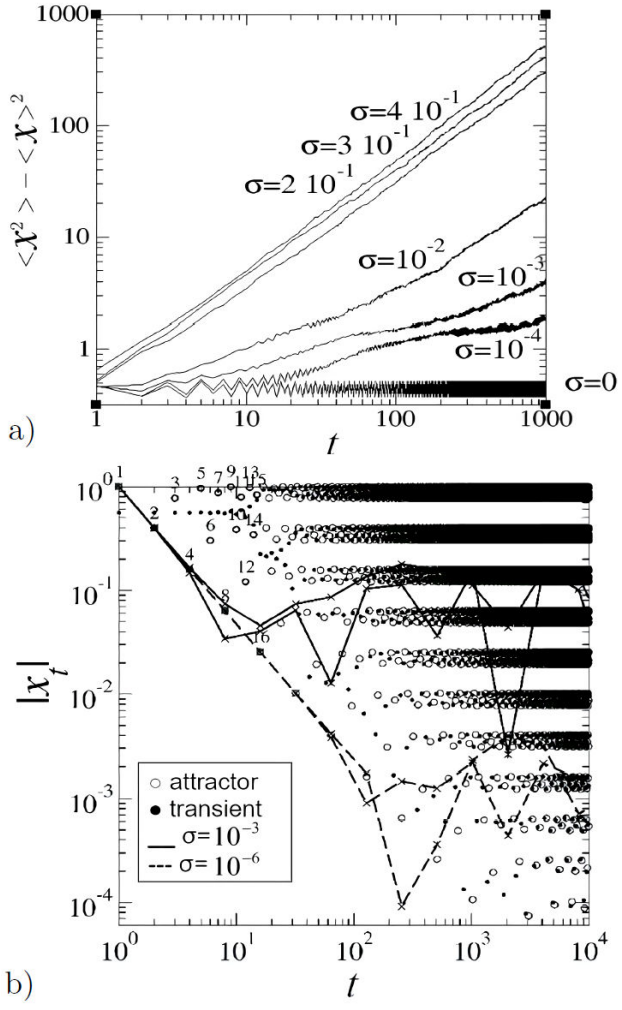

FIGURE 2. Glassy diffusion in the noise-perturbed onset of chaos. a) Time evolution of the mean square displacement for an ensemble of 1000 trajectories with initial conditions randomly distributed inside [-1,1]. Curves are labeled by the value of the noise amplitude. b) Absolute values of positions x_t in logarithmic scales for various trajectories at the onset of chaos $\mu_\infty(\sigma)$ starting at $x_0 = 0$. Open circles correspond to $\sigma = 0$ where the numbers label time $t = 1, ..., 16$. Solid (dashed) lines represent trajectories plotted only at times $t = 2^n$.

Diffusion was studied in the noise-perturbed map via a repeated-cell map where the map in each cell adapts the features needed from the quadratic map [15,16]. Trajectories can escape to neighboring cells and diffuse throughout only when $\sigma > 0$. The mean square displacement of such trajectories diminishes gradually as $\sigma \to 0$ and arrest takes place when $\sigma = 0$ since then all trajectories become finally confined into single cells. See Fig. 2a). Aging was noticed when studying trajectories [13,14] and their correlations [15,16] at the noise-perturbed onset of chaos $\mu_\infty(\sigma)$. Trajectories there recapitulate the structure of the bifurcation diagram with a noise gap, they initially resemble closely those of the noise-free case until a crossover time $t_\times = 2^{N(\sigma)}$ is reached after which they display superimposed randomness. See Fig. 2b). Actually, the master trajectory in Fig. 1b), $\sigma = 0$, exhibits perfect aging as this scaling property is exactly represented by the parallel diagonal position sub-sequences shown there. These positions can be exactly expressed as

$$x_{t+t_w} = \exp_q[-\lambda_q(x_{t_w})t/t_w], \tag{8}$$

where the waiting time t_w is $t_w = 2k+1, k = 0, 1, ...$, and q and λ_q are the same as above [13,14]. Trajectory correlations when $\sigma = 0$ behave similarly [15,16].

This robust analogy remained somewhat unexplained, suppression of diffusion and arrest due to cell escape-rate stoppage and aging scaling as a built-in feature. Recent work in progress is providing understanding and new perspectives. Glassy dynamics in molecular systems is visualized by a 'cage effect', where each molecule is effectively caged by its neighbors and can only move out when these neighbors cooperate with a chance opening. Relaxation to equilibrium requires concerted motions of increasingly larger groups of molecules as the temperature is lowered. When we consider an ensemble of trajectories in the Feigenbaum attractor instead of only one we get a parallel situation. If we place one initial condition at every point of the attractor, *i.e.* a uniform distribution, we observe the required concerted motion, since at every iteration a trajectory position x_t moves to the next position x_{t+1} that has been just left empty by another trajectory and the entire ensemble of trajectories moves jointly to the right in Fig. 1b). If the position at $x = 0$ is refilled at every iteration the distribution remains uniform. The addition of noise limits the size of concerted trajectory motion, and as we have said as a crossover phenomenon. The size of the groups of collaborative trajectories is dependent on the noise amplitude σ.

Some models for traffic flow have been constructed with nonlinear dynamical elements [68], while other studies of

traffic flow and arrest have found similarities with glassy dynamics [69]. The picture of a car-filled single or multiple lane road suggests itself. The noise-perturbed onset of chaos in quadratic maps puts together the ingredients of a basic model for traffic flow and jams. Additionally, the concerted dynamical evolution of an ensemble of trajectories at the noise-free period-doubling onset of chaos provides a concrete answer to the quest of the ideal glass.

2.3. Localizations

An equation can sometimes lead to a fruitful analogy. This was the case of a recursion relation involving matrix eigenvalues, that for those involved in the study had a specific meaning, but for others, outsiders would convey only its mathematical type. The recursion relation established the change in quantum transport properties between consecutive sizes of a model for arrays of wave scatterers [17]. But also that expression represented a specific dissipative nonlinear iterated map. The exploration of its bifurcation diagram, the nature of the attractors, the values of the Lyapunov exponent, and

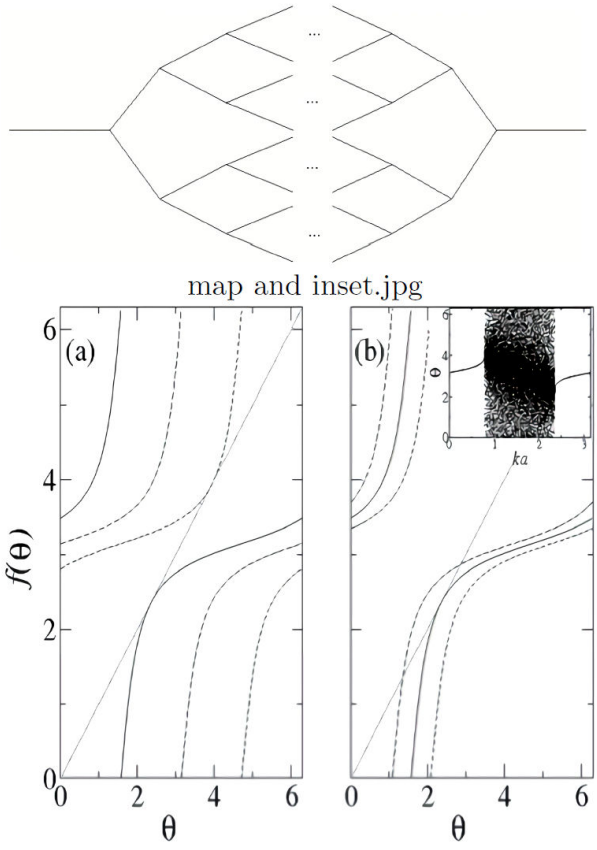

FIGURE 3. Top: A double Cayley tree of connectivity $K = 2$ and lattice constant a. Each bond is a perfect one-dimensional conductor. Bottom: a) The map transits (solid, dashed, and small-dashed lines) from tangency of the lower branch to tangency of the upper branch as ka varies. b) Detail where the lower branch changes from secant to tangent to off tangency. The dotted lines correspond to the identity. Inset: periodic and chaotic attractors.

other features, followed by their translation into electronic transport language, provided insight and a concrete original advance in the field, even though restricted to the limitations of a fully-solvable model [17].

Some specifics [17], The transport model is made of a lattice, a double-Cayley tree as shown in Fig. 3, of identical scatterers on its sites connected via perfect wires. The size of the system is measured by the generation n, the number of times the trees are ramified. Wave transport through this lattice was formulated via the scattering matrix method. Flux conservation, time-reversal symmetry, and lattice reflection symmetry implies that the 2×2 scattering matrix S_n has the form

$$S_n = \begin{pmatrix} r_n & t_n \\ t_n & r_n \end{pmatrix}, \tag{9}$$

where r_n is the reflection and t_n the transmission amplitudes. The matrix S_n can be diagonalized by a $\pi/4$ rotation, to yield two eigenvalues $\Lambda_1(n) = e^{i\theta_n}$ and $\Lambda_2(n) = e^{i\theta'_n}$, where θ_n and θ'_n are the eigenphases that satisfy $e^{\theta_n} = r_n + t_n$ and $e^{\theta'_n} = r_n - t_n$, so that $t_n = \frac{1}{2}(e^{\theta_n} - e^{\theta'_n})$. The dimensionless conductance depends on the eigenphases through the Landauer formula as $g_n = |t_n|^2$ [17].

The size of scattering matrix for the nodes S_{node} depends on the connectivity K of the Cayley tree and contains a single parameter ϵ, the transmission probability, a real number within $0 \leq \epsilon \leq 1/2$, that for convenience we use instead $\tau = \sqrt{1-2\epsilon}$. The other (tuning) parameter is the incoming energy ka, momentum k and lattice constant a. The recursion relation for the matrix S_n turns out to be [17]

$$S_n = -(e^{-2ika} I - \tau S_{n-1})^{-1} (\tau e^{-2ika} I - S_{n-1}), \tag{10}$$

where I is the identity 2×2 matrix, and from which the recursion relation for the phase θ can be extracted and reads [17]

$$f(\theta_n) = 2ka - \theta_n + \arctan\left(\frac{\sin\theta_n + \tau \sin 2ka}{\cos\theta_n - \tau\cos 2ka}\right). \tag{11}$$

The other eigenphase θ' behaves similarly.

The map $f(\theta)$ is shown in the panels a and b of Fig. 3 and its bifurcation diagram in the inset of panel b of the same figure. The attractors are of two types, there are two intervals of regular, period 1 sectors for small and large ka, separated by a sector of chaotic attractors. The attractors at the boundaries between the two kinds are transitions to chaos of the tangent bifurcation type [17]. The chaotic attractors exhibit intermittency. As shown in Fig. 3 the map is made of two branches that diverge when they meet. Depending on the value of ka either one branch or the other is closer to tangency with the identity line so that trajectories experience narrowing due to one branch followed by re-injection mediated by the other. Trajectories experience successive contractions and expansions leading to sub-exponential growth of sensitivity with iteration time (or system size) n characteristic of weak chaos [70], and the Lyapunov exponent vanishes [18]. Furthermore, this singular dynamics follows a Möbius transformation on the unit circle [18].

A complete transcription from nonlinear-dynamical to wave-transport languages can be established, the regular and chaotic regimes correspond, respectively, to the insulating gaps and conducting bands of the scattering system, and the tangent bifurcation transitions to and out of chaos to the mobility edges (of difficult access for many approaches in the field). There, the first vanishing of the Lyapunov exponent when entering the conducting band corresponds to the divergence of the localization length. Our previous determination (analytical and in closed form) of the sensitivity to initial conditions at the tangent bifurcation [6],

$$\xi_n = \exp_q(\lambda_q(x_0)n) \equiv [1-(q-1)\lambda_q(x_0)n]^{\pm\frac{1}{(q-1)}}, \quad (12)$$

with $q = 3/2$, became handy to obtain the conductance at the mobility edge of this model,

$$g_n \propto \left(1-\frac{1}{2}\lambda_{3/2}n\right)^{-4}, \quad (13)$$

with $\lambda_{3/2} = -2\sqrt{(1-2\epsilon)/2\epsilon}$ [17].

Wave propagation through scattering media when described by means of a double-Cayley tree permits full solutions as the Bethe lattice, a form of mean-field, often offers. Other physical situations where the localization phenomenon occurs, light, sound or elastic media wave scattering, can be likewise modeled and described by nonlinear dynamics of low dimensionality, with the underlying implication of a drastic reduction of degrees of freedom. This dynamics is represented by the Möbius transformation, the fixed points of which correspond to the localized states, and its ever-changing positions or phases to the extended states that display coherence due to vanishing Lyapunov exponent. Similar reductions of degrees of freedom leading to Möbius transformations have been observed in the synchronization of arrays of oscillators [71]. Incidentally, new directions for the modeling of collective behavior in complex systems, like swarms of small organisms, schools of fish or murmurations of starlings, could be based on coherent communication states resembling those described here for wave propagation.

3. Follow-ups

A claim about a novel kind of central limit stationary distribution for correlated variables to be displayed at the period-doubling onset of chaos attracted our attention and we examined sums of positions of trajectories. This initial effort led us to clarify the issue by uncovering a remarkable renormalization group picture. Unrelatedly, the consideration of an existing stochastic approach for the reproduction of ranked data pointed out a formal equivalence of a key mathematical expression with that for trajectories at the tangent bifurcation. This fact led to a nonlinear dynamical approach for rank distributions that shows similarities with universality classes in critical phenomena. Apropos, another instance involving the same mathematical expression came to our attention from an independent description of the dominant fluctuation in a model critical state. We elaborate on our immersion into this approach.

3.1. Sums

We consider sums of positions of trajectories generated by traditional nonlinear maps, like the quadratic (logistic) map. These are sums of deterministic variables as a difference with the ordinary case of sums of random variables produced by stochastic processes. For the latter kind, for independent identically distributed variables, the distribution of the infinite sum is the Gaussian, or normal, distribution as prescribed by the central limit theorem. Infinite sums of deterministic variables generated by fully chaotic maps lead also to the Gaussian distribution [72], but it was considered to be an open question whether such sums, when produced by attractors at or in the vicinity of a transition to chaos, would lead to a different outcome [73,74].

In our work [21-25] we considered sums of positions from a single trajectory and also from an ensemble of them, in the latter case started from a set of uniformly-distributed initial conditions along the interval of definition of the map. The chaotic-band attractors of the quadratic map are ergodic and therefore single and ensemble sums lead to the same limit distribution albeit the former sum takes more terms than the latter in resembling the final form [21,22]. At the transition to chaos, at μ_∞ in our chosen map, ergodicity is lost and the limit distributions are different.

The single trajectory at μ_∞ leads to a multifractal-valued sum, that once re-scaled is similar to the trajectory itself shown in Fig. 1b). The sum can be reproduced analytically and its distribution is an infinite set of delta functions as it has as support the mentioned multifractal sum [21]. It is totally different to the Gaussian distribution. For space shortness we show here the case of the sum of the absolute values of such positions, $y_{\mu_\infty}(N) \equiv \sum_{t=1}^{N} |x_t|$. See top block of Fig. 4, where the similarity of the centered sum

$$y'_{\mu_\infty}(N) \equiv \sum_{t=1}^{N}(|x_t| - c), \quad (14)$$

shown in panel C with the single trajectory in Ref. [21] can be appreciated. See Ref. [21] for the analytical derivation of $y'_{\mu_\infty}(N)$ and the expression for the centering constant c. See also in Ref. [21] the case of the natural sum $z_{\mu_\infty}(N) \equiv \sum_{t=1}^{N} x_t$.

We show in the panel d of the middle block of Fig. 4 the structure of the sum of positions of an ensemble of trajectories at μ_∞, $X(x_0, N; \mu_\infty) \equiv \sum_{t=0}^{N} x_t$, $-1 < x_0 < 1$. This structure can be understood [23] by considering the equivalent sum for the first few supercycle attractors, shown in the panels a, b, and c, for periods 2, 4, and 8, respectively, in the middle block of Fig. 4. The structure of the fractal function, which is this sum at μ_∞ as a function of the initial condition x_0, is built in stages that recapitulate the additional increasingly finer features added along the period-doubling cascade.

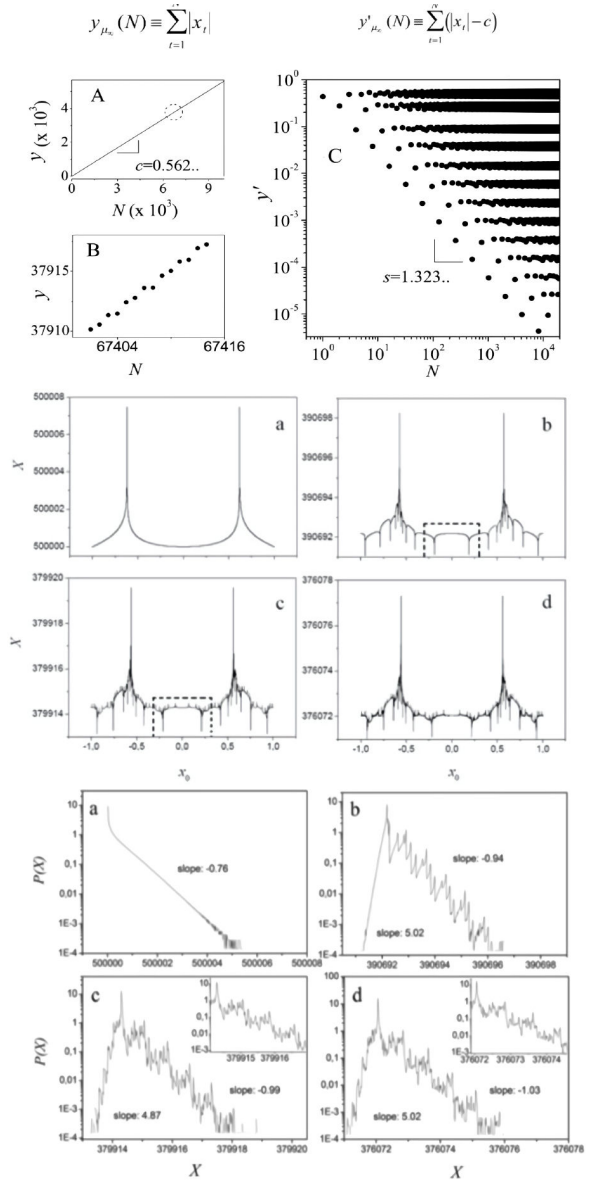

FIGURE 4. Top block: A) Sum of absolute values of visited points, x_t, $t = 0, ..., N$, of the Feigenbaum attractor with initial condition $x_0 = 0$. B) a closer look of the path of the sum, for values of N within the small circle in A. C) Centered sum $y'(N)$ in logarithmic scales. Middle block: Sums $X(x_0, N; \mu_\infty)$ as a function of x_0, $N \approx O(10^6)$ constructed by steps from period 2, 4 and 8 supercycles, and finally at the Feigenbaum point. Bottom block: Histograms obtained from the sums above.

The corresponding distributions are shown in the bottom block of Fig. 4, where we observe again the development of a fractal function [23].

When $\mu > \mu_\infty$ the evolution of the distribution of sums of positions, of a single trajectory, or of an ensemble of them, inevitably takes the stationary Gaussian form as the number of terms $N \to \infty$. This can be rationalized [21] when recalling that dynamics inside a 2^K-band attractor, $K = 1, 2, ...$, can be decomposed into inter band periodic motion of period 2^K (as in the corresponding periodic attractor) and intra band chaotic motion. That is, every position x_t can be decomposed as arrival at the 'center' $\bar{x}_t$ of a band and a shift δx_t within the band, $x_t = \bar{x}_t + \delta x_t$. Therefore the sum $z_\mu(N) \equiv \sum_{t=1}^{N} x_t$ can be split into two terms $z_\mu = \bar{z}_\mu(N) + \delta z_\mu(N)$ where $\bar{z}_\mu(N) = \sum_{t=0}^{N} \bar{x}_t$ and $\delta z_\mu(N) = \sum_{t=0}^{N} \delta x_t$. The intra band shifts behave as independent random variables and the limiting distribution of their sum is Gaussian. The inter band motion is completely correlated but this contribution is increasingly eliminated when the number of terms in the sum increases as $N \to \infty$. The values of the total sum, initially within the chaotic bands, fall into increasingly wider bands that merge into a single one according to the mean-square displacement $\langle [\delta z_\mu(N)]^2 \rangle^{1/2} \approx N^{1/2}$ [21].

Remarkably, the overall picture can be cast into a renormalization group scheme where the operation is the sum of positions and this leads to only two fixed points. The nontrivial corresponds to the multifractal distribution at $\mu = \mu_\infty$ while the trivial one is that prescribed by the ordinary central limit theorem [21,22]. When $\mu > \mu_\infty$ the flow towards the trivial fixed point displays a crossover behavior [21,22], the fine details of which and other relevant issues were resolved numerically [24] by considering the family of attractors at chaotic-band-splitting or Misiurewics points. As it turned out [25] the distribution at the crossover is related to incomplete sampling of data and therefore resembles the so-called T-Student distribution, that can in turn be rewritten into the form of a q-Gaussian distribution [73,74]. At the present date, this research line focuses on a specific model of correlated walks that displays anomalous diffusion and arrest.

3.2. Rankings

A clear-cut stochastic approach [75] to obtain theoretical size-rank functions $N(k)$ considers samples for the magnitudes N of unspecified kinds of data to be represented by sets of random values generated by a parent or source distribution $P(N)$. When $P(N)$ is chosen to be the power law $P(N) \approx N^{-\alpha}$, $\alpha > 1$, one obtains [75,27]

$$N(k) = N_{\max} \exp_\alpha [-N_{\max}^{\alpha-1} \mathcal{N}^{-1} k], \qquad (15)$$

where $N_{\max}$ is the largest data value (with initial rank $k = 0$) and $\mathcal{N}$ is the total number of data in the sample. Moreover, when $N_{\max} \to \infty$, a pure power-law decay follows, $N(k) \propto k^{1/1-\alpha}$, $\alpha > 1$. And when $\alpha = 2$ it takes the 'classical' Zipf form $N(k) \propto k^{-1}$.

Now, a very different situation is the, longtime established nonlinear-dynamical, problem of determination of a functional-composition renormalization-group fixed-point map for a transition to chaos such as, for example, the tangent bifurcation [76,3]. This is to find the function $f^*(x)$ (and the value of ζ) that is the solution of $f^*(x) = \zeta f^*(x/\zeta)$, such that it also complies with the generic form for a map at tangency when x is small, $f^*(x) = x + u|x|^z + ...$ The solution is [76,3]

$$f^*(x) = x \exp_z(u x^{z-1}), \zeta = 2^{1/(1-z)}, \qquad (16)$$

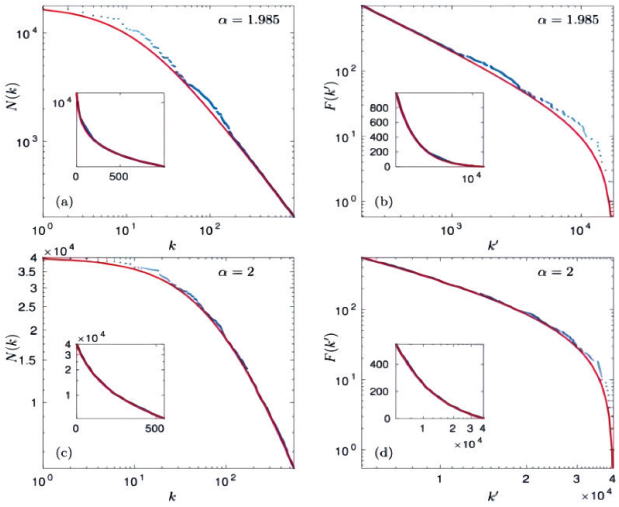

FIGURE 5. Data fitting. Earthquakes (top) and forest fires (below) [31]. Size-rank $N(k)$ and frequency-rank $F(k')$ distributions are inverse functions [31]. As indicated, the values of α needed for fitting are close to $\alpha = 2$ that for the classical Zipf law.

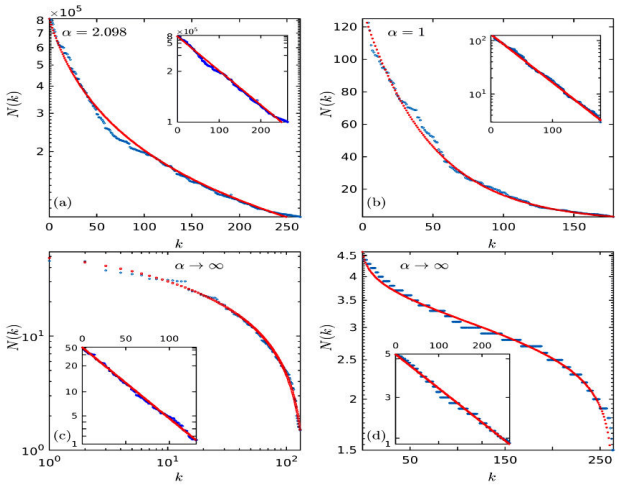

FIGURE 6.Data fitting. Examples of four different universality classes [32]: a) USA city populations. b) Infant mortality per country. c) Fireams owned per 100 capita and per country. d) Los Angeles household sizes.

a map with the scaling property, that reflects on the fact that all its trajectories obey the form [27]

$$x_t = x_0 \exp_z(|x_0|^{z-1} u t). \tag{17}$$

For convenience we consider now only trajectories started at the left of the point of tangency $x = 0$, for which all values of $x_t < 0$.

Equations (15) and (17) are identical, one transforms into the other through the equivalences $k = t$, $N(k) = -x_t$, $N_{max} = -x_0$, $\alpha = z$ and $\mathcal{N} = u^{-1}$. Remarkably, size-rank distributions $N(k)$ for all power-law exponents α can be reproduced by trajectories of the fixed-point map $f^*(x)$ [27]. And as it turns out also for $\alpha \to \infty$. More generally, $N(k)$ for all source distributions $P(N)$ can be obtained from trajectories of the map $x' = x + u/P(-x)$ under the same scheme [32]. The stochastic and the deterministic approaches are equivalent. This duality permits for an explicit and quantitative distinction between size-rank $N(k)$ -sizes of cities- and frequency-rank $F(k')$ -word frequencies- distributions, as the former appears as a trajectory while the latter is a sum of positions [31]. The frequency-rank distribution $F(k')$ turns out to be the functional inverse of $N(k)$ [31]. See Fig. 5.

There are other surprising sets of properties related to this topic that can be obtained from the map at tangency. The reciprocals of $N(k)$ provide uniformly-distributed probabilities $p^{(k)}$ for each k that lead to extensive q-deformed entropies where system size is measured by sample size $k_{max} = \mathcal{N}$ [29,30]. We have $S_{2-q}(k_{max}) = \ln_{2-q}[p^{(k_{max})}/p^{(k=0)}] \sim \mathcal{N}, q = z = \alpha$. The numbers $N(k)$, we recall, were obtained from trajectories, with $x_t < -1, t = 0, 1, ..., t_{max}$, from the $x < 0$ branch of the map. Therefore the probabilities $p^{(k)}$ can be obtained as trajectories, with $x_t < 1, t = 0, 1, ..., t_{max}$, from the $x > 0$ branch of the map [29,30]. Also, trajectories from that same branch, starting and running now with $x_t \geq 1$, $t = 0, 1, ...$, generates the most renowned sets of numbers (or increasingly better approximations of them). Fibonacci numbers when $z = 1$, Natural numbers when $z = 2$, Prime numbers when $z = 2$ with logarithmic corrections, Factorial numbers when $z \to \infty$. In turn, the negative reciprocal of these numbers appear as trajectories from the $x < 0$ branch of the map with $x_t > -1, t = 0, ..., \infty$. The series formed by these reciprocals converge for $z < 2$ but diverge for $z \geq 2$, in fact, the borderline for divergence manifests as $z = 2$ with logarithmic corrections, related to the known bounds for the Prime numbers and the very slow divergence of their reciprocals. This is reminiscent of borderline dimensionality and its logarithmic corrections in critical phenomena. (At the moment of writing this review this material is in preparation for publication).

We have collected real data cases and reproduced their size-rank distributions $N(k)$ quantitatively from our approach. Infant mortality with $\alpha = z = 1$; billionaires, solar flares, California forest-fire areas, and USA city populations with $\alpha = z = 2$; earthquake magnitudes with $\alpha = z = 2$ plus logarithmic corrections; and gun ownership with $\alpha = z \to \infty$ [29,31,32]. See Figs. 5 and 6. So, this is evidence that ranked data appear to be represented by the universality classes to be distinguished by the above values for $\alpha = z$. Interestingly, the nonlinear maps, all of the fixed-point kind $f^*(x)$ already described, have all a tangency feature, when $z = 1$ the map crosses the identity line, for $z = 2$ the map is tangent, and it is regular with nonzero second derivative or curvature $u > 0$, in the limit $\alpha = z \to \infty$ the tangency point shifts to infinity [32]. Also, the finite size effect of real data is resolved by taking the matching map off tangency [32].

Moreover, the expression for $N(k)$ is a q-deformed exponential, the reciprocal of which is also a q-deformed exponential but with index $Q = 2 - q$ or $\alpha' = 2 - \alpha$ or

$Z = 2 - z$. When $q = \alpha = z = 1$ the ordinary exponential ($N(k)$) and its functional inverse the ordinary logarithm ($F(k')$) are far from each other separated by all power-law decay functions. As $q = \alpha = z$ grows away from unity the q-deformed exponential and logarithmic functions develop a closer resemblance as they both have power-law decay. When $q = \alpha = z = 2$ their power-law decay is identical (explaining the usage for both $N(k)$ and $F(k')$ as Zipf law). There, $Q = \alpha' = Z$ vanishes. The number $Q = \alpha' = Z$ has been shown to represent a 'contraction' dimension, an index that quantifies the reduction of phase space exerted by an attractor [29,30]. For a chaotic attractor $Q = \alpha' = Z = 1$, for a multifractal attractor $Q = \alpha' = Z < 1$, and for a periodic attractor (including a tangency point) $Q = \alpha' = Z = 0$. Thus, for all $q = \alpha = z > 2$ the contraction dimension must remain zero. Within this scheme, the Zipf law appears at a borderline dimension similar to those in critical phenomena, and curiously represented by the set of Prime numbers.

3.3. Fluctuations

An interesting set of studies [77,78] for the spatial structure and temporal evolution of fluctuations at a typical critical state made use of the Landau-Ginzburg-Wilson (LGW) effective Hamiltonian together with an inferred nonlinear iterated map near tangency. Detailed results were obtained for the dominant fluctuation, a large long-lived object obtained via the saddle-point approximation, as is usual in statistical mechanics. For the one-dimensional case the resultant order parameter profile $\phi(x)$ expression can be rewritten as [33]

$$\phi(x) = \phi_0 \exp_q(\phi_0^{q-1}\sqrt{2b}x), \tag{18}$$

where ϕ_0 is the amplitude at the middle of the fluctuation of length $2R$, $q = (1+\delta)/2$, with δ being the critical isotherm exponent and b a leading Hamiltonian parameter. It can be noticed immediately that Eq. (18) is identical to Eq. (17) with the identifications $x = t$, $\phi(x) = x_t$, $\phi_0 = x_0$, $q = z$ and $\sqrt{2b} = u$. Furthermore, the time evolution of such fluctuations were put forward to be of the intermittent type, gradual growth (in amplitude or size) until collapse followed by the appearance of a new fluctuation, and so on [78]. This sequel would be delivered by a nonlinear map just off tangency followed by a cusp feature responsible for re-injection to the left of the bottleneck.

So, we were presented with another plausible instance where the renormalization-group fixed-point map $f^*(x)$ at the tangent bifurcation would play a main role. And, more generally, the possibility of unanticipated connections between the field of critical phenomena in statistical mechanics and anomalous nonlinear dynamics at the transitions to chaos, a setting where generalized q-deformed entropy expressions appear naturally. A powerful method for the study of inhomogeneous systems is the (Free energy) density functional theory and within this a frequently used functional is that related to the so-called square-gradient approximation, a version of which is the LGW Hamiltonian

$$\Psi_c[\phi] = a \int dr^d \left[\frac{1}{2}(\nabla\phi)^2 + b|\phi|^{\delta+1}\right]. \tag{19}$$

However, the object of study, the dominant fluctuation, differs from the mainstream output in that it is not an equilibrium structure.

The vanishing of the first variation of the above free energy functional, or Euler-Lagrange equation, turns out to be analogous to the second law for a classical-mechanical particle [33,35], with positions ϕ, at times x and under a potential of force $V = -b|\phi|^{\delta+1}$. This analogy makes it possible to determine the possible types of order parameter profiles $\phi(x)$ for the dominant critical fluctuation, for example, via the corresponding phase portrait

$$\frac{d\phi}{dx} = \pm\sqrt{2(U + b|\phi|^{\delta+1})}, \tag{20}$$

where U is the 'total energy', the constant arising in the first integration of the Euler-Lagrange equation. There are two types of particle trajectories or profiles, antisymmetric and symmetric with respect to their midpoint such that the force exerted at their boundaries differs in sign, and this determines whether the fluctuation grows or shrinks [35]. See Fig. 7. The expression for the particle trajectory $\phi(x)$ for vanishing total energy $U = 0$ corresponds to that in Eq. (18) [33,35]. The fluctuation size or particle's time of flight diverges for $U = 0$.

Interestingly and also helpfully, the calculation of the second variation of the free energy functional leads to another mechanical analogy, this time with a quantum particle. The second variation expression has the form of a Schrödinger

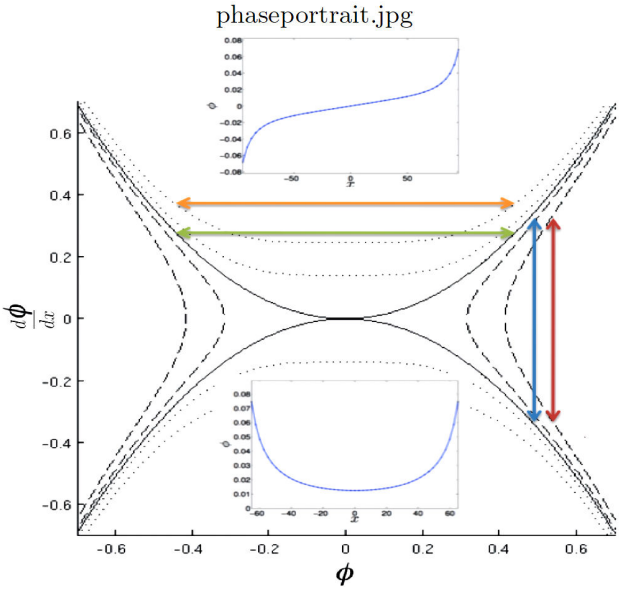

FIGURE 7. Phase portrait from Eq. (20) for different values of the total energy U. The insets show the 'trajectories' or order-parameter profiles ϕ that correspond to the horizontal and vertical arrows.

equation such that the associated eigenfunctions correspond to perturbations of the order parameter profile while the eigenvalues indicate the stability of the profile to such perturbations [35]. We recall that the profile $\phi(x)$ describes an unstable statistical-mechanical object and therefore some eigenvalue must be negative or at least vanish [35].

Similarly to the previous Section, extensive q-deformed entropies can be obtained, this time from the order parameter value at $x = R$, $\phi(R) = \phi_0 \exp_q(\phi_0^{q-1}\sqrt{2b}R)$, as this provides a measure of the dependence of configuration numbers on fluctuation size R [33-35]. We have $S_q(R) = \ln_q(\phi(R)/\phi_0) \sim R$. For a classical critical point $\delta = 3$ so that q takes the ubiquitous value $q = (1+\delta)/2 = 2$, whereas for an ordinary state off criticality $\delta = 2$ one recovers the ordinary case $q = 1$ [33-35].

Time evolution via density functional theory is provided, phenomenologically, via a class of first order but nonlinear differential equations of which the Landau equation

$$\frac{d\phi}{dt} = -A\frac{\delta\Psi_c[\phi]}{\delta x} \simeq -B\frac{d\phi}{dx}, \phi \simeq 0, \qquad (21)$$

here with A and B constants, is prototypical. Time evolution ends up when $\delta\Psi_c[\phi]/\delta x = 0$, and the Euler-Lagrange equation delivers a stationary profile. Use of the phase-portrait expression in Eq. (20) yields

$$\frac{d\phi}{dt} = \mp B\sqrt{2(U + b|\phi|^{\delta+1})}, \phi \simeq 0. \qquad (22)$$

And the above equation becomes, after introduction of discrete time and the choice $U = 0$,

$$\phi_{t+1} = \phi_t + B\sqrt{2b}|\phi_t|^{(\delta+1)/2}, \phi \simeq 0, \qquad (23)$$

a map that has the common local tangency form $f(x) = x + u|x|^z$, $x \simeq 0$, we have considered above for the discussion about the renormalization group fixed-point map $f^*(x)$ in Eq. (16). This time $x = \phi$, $u = B\sqrt{2b}$, and $z = (\delta+1)/2$. The map $f^*(x)$ can be perturbed and taken off tangency revealing two branches joined by a cusp [35]. The resulting trajectories exhibit intermittency, that is, sequels of laminar episodes (passage through a bottleneck) separated by bursts (reinjections mediated by the second branch) [35]. Perturbation in the opposite direction leads to fluctuation collapse [35]. See Figs. 8a) and 8b).

In relation to the previous Subsection, Rankings, it is worthwhile to mention that some of the properties of dominant fluctuations, basically obtained through the saddle-point approximation in a coarse-grained partition function, can be also obtained considering a phenomenological scheme based on sub-occupation of ϕ-phase space [34,28].

Current interest in this problem is directed towards the determination of early warning signals for the final stage of the long-lived but finite lifetime of the dominant critical fluctuation.

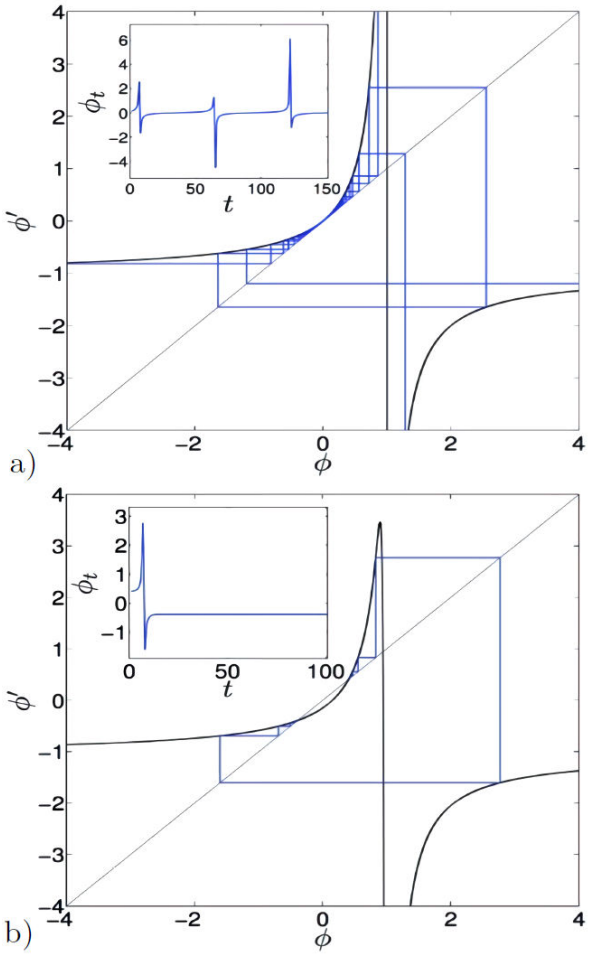

FIGURE 8. Intermittency a) and collapse b) of fluctuations as described by the perturbed fixed point map.

4. Rehearsals

An invitation to join the exploration of a novel algorithm to transform time series into networks consisted of considering trajectories representative of the three routes to chaos in low-dimensional nonlinear systems. This effort led to connections between renormalization group schemes and entropy optimization, and also a re-encounter with generalized Pesin identities. Unconnectedly, a program to revisit the well-known properties of families of attractors of the quadratic map as seen through the densities of ensembles of trajectories ran into a surprising statistical-mechanical picture. Another case study consisted of the inspection of the consequences of introducing discrete time to the replicator equation for a collection of well-known (social) games. We were headed straightforwardly into a nonlinear-dynamical extension of evolutionary game theory.

4.1. Networks

The Horizontal Visibility (HV) algorithm [79] transforms real-valued time series x_i, $i = 0, 1, 2, ...,$ into connected

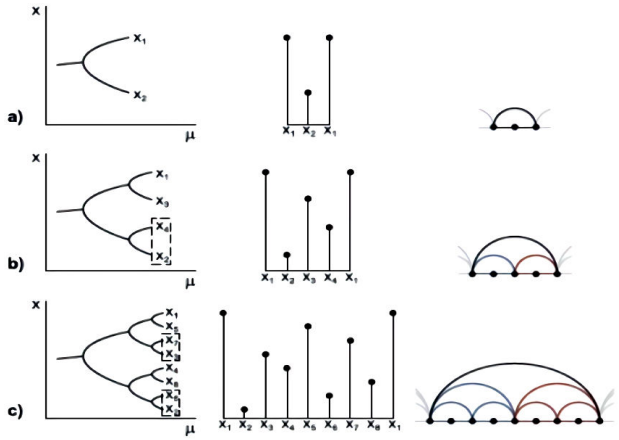

FIGURE 9.Illustration of the HV algorithm that converts time series into a graph that shows the HV motifs for period doubling.

graphs that contain always as 'backbone' a simple chain graph. See Fig. 9. The algorithm assigns a node i to each datum x_i and links pairs of nodes (i,j) only when (x_i,x_j) fulfills the criterion, $x_i,x_j > x_l$, for all l between i and j, $i<l<j$ [79]. By construction large families of time series share the same HV graph, as there are infinitely many near-valued time series that match the HV criterion in the same sequential manner. The families of trajectories produced by attractors of prototypical nonlinear iterated maps represent a category of time series onto which the HV algorithm can be straightforwardly applied. Since knowledge about their properties, *e.g.* along the established routes to chaos, has substantially accumulated and developed over the years, they offer an ideal case to evaluate the algorithm, either by its capacity to capture previous knowledge in a different format or because it facilitates the generation of new knowledge.

We applied the HV algorithm to representative trajectories inside the attractors along the period-doubling and chaotic band-splitting cascade of the logistic map [36,37]. And also to trajectories along the quasi-periodic routes to chaos for the metallic irrational numbers (such as the golden and silver ratios) of the circle map [39]. Additionally, we determined the HV graphs for the tangent bifurcation at the edge of the period-three window of the logistic map and its chaotic neighborhood where intermittency of Type I occurs [40]. These implementations allowed us to observe the development of interesting invariant HV network structures at these well-known transitions to chaos. See Fig. 10. Also significantly, we obtained analytical expressions for their degree k distributions $P(k)$. These distributions show truncated exponential decay with k along the period-doubling family of attractors [36,37]. For period 2^n

$$P(n,k)=\begin{cases}\left(\frac{1}{2}\right)^{k/2} & k=2,4,6,...,2n,\\ \left(\frac{1}{2}\right)^{n} & k=2(n+1),\\ 0 & k>2(n+1).\end{cases} \tag{24}$$

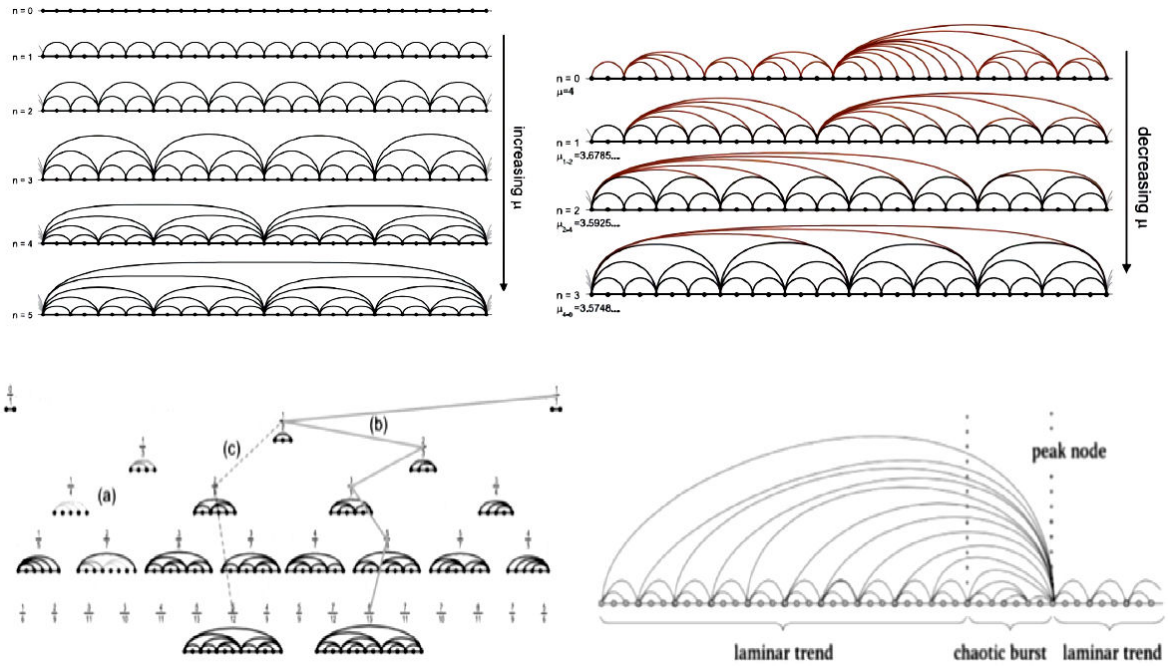

FIGURE 10. Top: Sequence of HV graphs for the period-doubling and chaotic-band splitting cascades. Bottom left: Periodic attractor HV motifs a) associated with the rational fractions p/q along six levels of the Farey tree. b) Five steps into the Golden ratio route, $b=1$ (thick solid line); c) Three steps into the Silver ratio route, $b=2$ (thick dashed line). Bottom right: Illustration of an HV graph for Type I intermittency extracted from the period-three tangent bifurcation in the logistic map.

The degree distribution $P(n,k)$ for 2^n-band chaotic attractors is similar to that in Eq. (24) except that there are nodes with degree $k \geq 2(n+1)$ arising only from the top band, as the algorithm filters out chaotic motion within all bands except for that at the top. This contribution decreases as $n \to \infty$, leading in the limit to a full exponential distribution. A similar result was obtained for the quasi-periodic metallic number cases [39],

$$P(n \to \infty, k) = \begin{cases} \phi_b^{-1} & k = 2, \\ 1 - 2\phi_b^{-1} & k = 3, \\ (1-\phi_b^{-1})\phi_b^{(3-k)/b} & k = bn+3, \\ 0 & \text{otherwise}, \end{cases} \tag{25}$$

where the metallic numbers ϕ_b are those irrational numbers with pure continued fraction $[b,b,b...], b = 1(\text{gold}), 2(\text{silver}), ...$, and for which the attractor periods approximate the numbers ϕ_b^n as n increases. As a difference, the degree distribution $P(k)$ at the tangent bifurcation decays as a power law [40].

The structure of the HV networks obtained from attractor trajectories lends itself in all cases to the consideration of a simple (contiguous-node-merging) renormalization-group transformation [36,37,39,40]. For the logistic map there are two trivial fixed-point HV graphs, those from period one (single chain) and from a single chaotic band (single chain dressed with random links), and one nontrivial fixed-point (scale-invariant) graph, that for the transition to chaos [36,37]. Parallel results were obtained for the same node-merging operation on the HV graphs when applied along the quasi-periodic and intermittency routes to chaos [39,40]. The ingredients for a test of a previously considered ide a [80] were in place. This is that that there is a hidden entropy optimization procedure underlying the renormalization group technique, developed to obtain quantitative results for systems with scale-invariant properties. Specifically, that the all-important trivial and nontrivial fixed points are extrema of a suitably defined entropy. From the degree distributions $P(k)$ there is access to entropy through the Shannon expression. The results were positive for all cases: period doubling and chaotic-band splitting cascades and their common accumulation point [36,37], quasi-periodic routes to chaos [39], and the tangent bifurcation together with its chaotic neighborhood [40].

The scale-invariant HV graphs obtained from the trajectories at the transitions to chaos themselves, the nontrivial fixed-points in the previous comment, are no longer made of repetitions of motifs like those for the periodic attractors (see Fig. 10), as the size of the motif has grown to infinity. The examination of their network structure, their degree distribution and their entropy expressions produced another significant result: the occurrence of an HV network version of the q-generalized Pesin identity at the period-doubling [38] and the quasi-periodic [41] transitions to chaos, described earlier in Subsection IIA, Sensitivities. In both cases, the 'distillatory' quality of the HV algorithm, many time series into one graph, simplifies the multifractal set at the transition to chaos attractor into a fractal set. This advance required the network generalizations of sensitivity to initial conditions and of Lyapunov exponent. Currently, activity in this topic is centered on the global statistical-mechanical structure of families of HV networks along all the quasi-periodic routes to chaos that comprise the set of all irrational numbers in the unit interval.

4.2. Measures

Recently, we undertook the seemingly unnecessary task of revisiting the known properties of the logistic map in Eq. (1), but not by reproducing trajectories and their attractors by running through the values of the control parameter μ across its full interval $[0,2]$. Instead, we were interested in observing these properties via the density distributions $\rho_t(x;\mu)$ of ensembles of trajectories as they evolve in time t and see how they settle into their invariant forms for $t \to \infty$. The difference between these two viewpoints is similar to that familiar in the representations of particle diffusion, one of them describes the evolution of single particles via the Langevin equation while the other follows the probability density of all the particles via the Fokker-Planck equation [81]. The statistical mechanical understanding can be increased [82] by this dual endeavor, where the place of the Fokker-Plank equation is taken here by the Frobenius-Perron equation [83].

More specifically, we considered [43] two families of attractors, the supercycles along the period-doubling cascade and the Misiurewics points along the chaotic-band-splitting cascade, together with their common accumulation point at the transition to and out of chaos. When the Frobenius-Perron equation is particularized to the logistic map reads [43]

$$\rho_{t+1}(x;\mu) = \frac{1}{2\sqrt{\mu(1-x)}} \left[\rho_t(y) + \rho_t(-y)\right], \tag{26}$$

where $y = \sqrt{(1-x)/\mu}$. While the reverse time evolution follows [43]

$$\rho_{t-1}(x;\mu) = \begin{cases} \mu x \rho_t(1-\mu x^2), & x \in [0,1], \\ -\mu x \rho_t(1-\mu x^2), & x \in [-1,0]. \end{cases} \tag{27}$$

We found that the approach of the densities to the final invariant limit, the invariant measure, is fast and that the development and shape of the distribution is very similar for periodic and chaotic-band attractors. See Figs. 11a) and 11b) [43] where we have considered uniformly-distributed initial conditions throughout the interval $[-1,1]$. Interestingly, the approach to the invariant distributions follows a precise concerted sequence for both periodic or chaotic attractors. The developments of the distributions for period or number of bands 2^n imitate closely those for all smaller periods or numbers of bands, appearing around iteration times $t \sim 2^k, k = 1,2,...,n-1$. We refer to this property as 'recapitulation'.

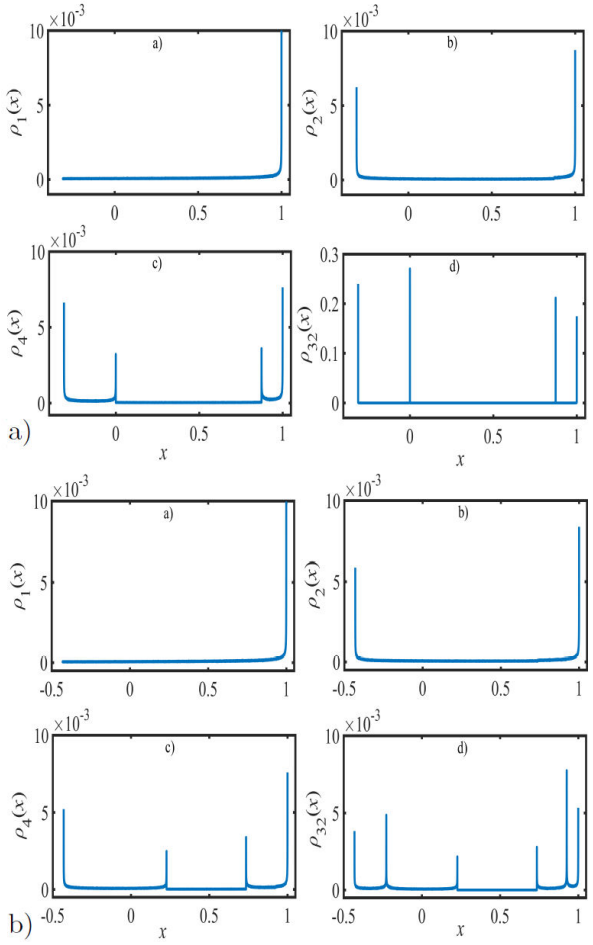

FIGURE 11. a) Evolution of an initially uniform density of positions in the interval [-1,1] for the supercycle of period 4. b) Same as a) but for the Misiurewics point when 2 chaotic bands are about to split into 4 bands.

It is instructive to mention that invariance of the distributions in the limit $t \to \infty$ is only observed at times of the form $t = M2^n$, M a large positive integer, when the ensemble of trajectories is (technically) inside the attractors. That is, the limit densities follow the known dynamics for the order of visits of positions or bands. Two different time scales develop, t and n, and these separate increasingly as $n \to \infty$. For the particular case when the initial distribution of positions is already the invariant distribution time separation of scales is not observed though, dynamically, the order of visits of positions is always taking place.

As expected another renormalization group scheme became promptly visualized [43] since the families of invariant densities are linked by a self-affine property, just as their attractors do in the bifurcation diagram (μ, x). On this occasion, the renormalization group operation on the densities is simply period halving or band merging followed by rescaling. The trivial fixed points are a single delta function for period one and the bathtub-shaped density for single-band chaos, $\rho_\infty(x;2) = (\pi\sqrt{1-x^2})^{-1}$. The nontrivial fixed point is a multi-delta function distribution with multifractal support [43].

With the families of densities in hand, the opportunity of evaluating their entropies from Shannon's expression was an uncomplicated task. First of all, the fixed points could again be identified from entropy optimization. For period one the entropy vanishes reaching its minimum possible value, while the entropy for the single chaotic band attains the maximum value. The entropy for the nontrivial fixed point at the transition to chaos is maximum for all supercycles and minimum for all Misiurewics points. Secondly, the entropy of the invariant densities grows monotonically from period one through all supercycles, and all Misiurewcs points to the final single-band attractor [43].

But most remarkably, when the collection of entropies for the two families of attractors is viewed along the values of control parameter μ the familiar pattern appears [43] of a statistical-mechanical two-phase system separated by a continuous phase transition, an equation of state containing a critical point. Similar, for example, to that typical for an order parameter as a function of temperature for zero external field. Where the role of temperature is taken by the control parameter.

A few decades ago, it has been a common general commentary within the Complex Systems community that observations of complex systems in nature appear to indicate, in the language of nonlinear dynamics, that their conduct is as if they evolve at the 'edge of chaos'. Likewise, the same community nowadays shares the general commentary that the observations of complex systems in nature seem to imply, in the language of statistical mechanics, that they thrive in a state of 'criticality'. Amusingly, as we describe here, these two paradigms appear to be equivalent at the transition to chaos displayed by the archetypal nonlinear dynamical model.

4.3. Games

Game theory is a widespread theoretical tool in the modeling of complex systems, that under consideration of many degrees of freedom, or agents, provides time processes, altogether referred to as evolutionary dynamics [84]. The agents interact and reproduce according to the result of their interaction, which in turn depends on the composition of the population. The prediction of the final population compositions, or Nash equilibria, is of interest. Under the 'well-mixed' version, where agent interactions occur randomly, similar to mean-field approximation in statistical mechanics, the task centers in a set of first-order nonlinear differential equations called the replicator equations [84]. In vector notation, these equations read

$$\dot{x}^i = x_i \left[(A\mathbf{x})_i - \mathbf{x}^T A\mathbf{x} \right], \tag{28}$$

where x_i is the frequency of type $i = 1, ...n$, $\mathbf{x}$ is the frequency vector describing the population as a whole, the interaction is given by the nxn payoff matrix A. $(A\mathbf{x})_i$ is the expected payoff for an individual of type i and $\mathbf{x}^T A\mathbf{x}$ is the average payoff of the population.

We focused attention on the simplest option, the well known social-dilemma (two-strategy, cooperation or defection,) games represented by symmetric 2x2 payoff matrices that lead to a single differential equation $dx/dt = x(1-x)[S + (1-T-S)x]$, where x stands for the proportion of cooperative strategists in the population (and $1-x$ that for defection strategists). The values of the payoff matrix parameters S and T define four basic social dilemmas: When $T > 1$ and $S > 0$ we have the Snowdrift game (also known as Chicken or Hawk-Dove); the choice $T < 1$ and $S < 0$ corresponds to the Stag Hunt game; the range $T > 1$ and $S < 0$ is for the Prisoner?s Dilemma game where defection is the best option no matter what the opponent chooses; and finally the option $T < 1$ and $S > 0$ corresponds to the Harmony game, with cooperation being now the best strategy. See Ref. [44].

The appearance of chaotic dynamics in these games is ruled out by the Poincare-Bendixon theorem that establishes that chaos can only arise in a continuous dynamical system (specified by differential equations) if it has three or more dimensions. Therefore we chose to introduce discrete time into the replicator equation and convert it into a nonlinear iterated map with two control parameters S and T,

$$x_{t+1} = x_t + x_t(1-x_t)[S + (1-T-S)x_t], \qquad (29)$$

and embark on the program of exploring the mentioned social games through the bifurcation diagram of the map in Eq. (29).

The results were immediate, the landscape of the three-dimensional (S, T, x) bifurcation diagram uncovers a rich arrangement of periodic and chaotic attractors connected by recognizable but somewhat distorted period-doubling and chaotic band splitting cascades, windows of periodicity, etc. [44]. See Fig. 12a) where the values of the Lyapunov exponent on the (S, T) plane are shown through color variation. A cut along the line $A = S = T$ is shown in Fig. 12b) where one can see two disconnected sets of attractors for $A < 0$ and modified interiors in the, more visible, window of period three.

Surprisingly for us, the same replicator map in Eq. (29) was obtained after a major reduction [46] is made on a game-theoretic adaptation [85] of the Tangled Nature (TaNa) model [86] for evolutionary dynamics of ecological systems. The game-theoretic version of the TaNa model consists of a large payoff matrix so that the replicator equation involves a large frequency vector [85]. This model exhibits macroscopic non-stationary intermittent evolution similar to that in the TaNa model, and, interestingly, its discrete-time version that operates in the limit of many strategies constitutes a coupled map lattice (CML). Subsequently, a drastic simplification of these CML replicator-mutation equations was considered to reduce the model all the way down to a one-dimensional nonlinear map [46]. With this approximation, the possible connection was examined between the macroscopic intermittent behaviors of the above-mentioned high-dimensional models with the known low-dimensional sources of intermittency, such as

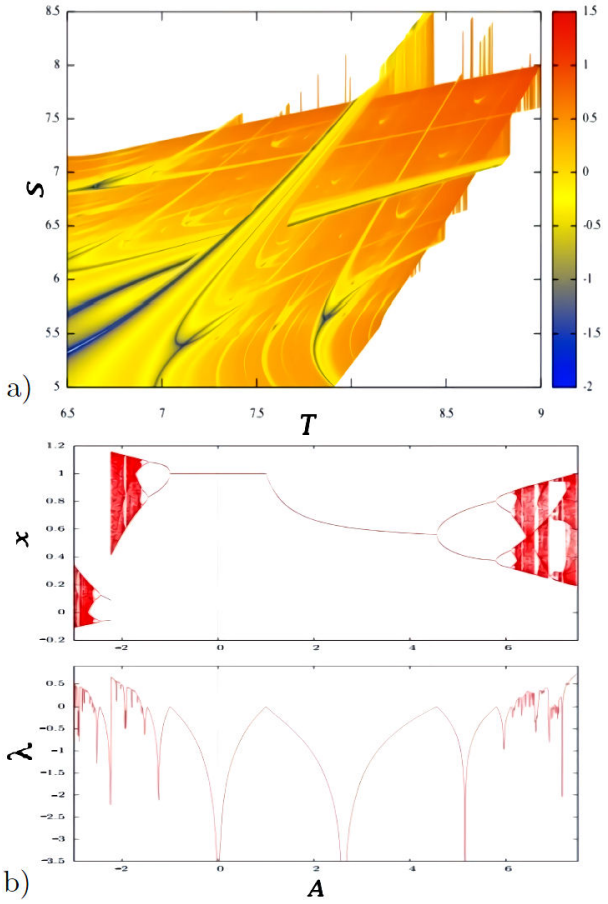

FIGURE 12. a) Lyapunov exponent in control parameter plane (S,T) (blue indicates negative and yellow/orange positive values. b) Bifurcation diagram and Lyapunov exponent along the parameter line $A \equiv S = T$.

the tangent bifurcation. In short, the many-strategy game-theoretic problem was reduced to a classic version of two strategies, where one of them represents a selected agent or species and the other groups all the others. One advantage in using this approximation is that a one-dimensional nonlinear dynamical model had been recently constructed [45] such that its time evolution consists of successive tangent bifurcations that generate patterns resembling those of the full TaNa model in macroscopic scales. See 13b) and d).

Currently, we are modifying, phenomenologically, the replicator map in Eq. (29) such that different desired features in its original bifurcation diagram occur within the physical interval $0 \leq x \leq 1$, and can, therefore, be incorporated in specific model constructions. One example is a game that replicates Yule's principle ('rich get richer') [87], that in network language terms corresponds to 'preferential attachment' [88].

5. Belated insights

We computed properties of ensembles of trajectories evolving towards (first periodic and then chaotic) attractors of the

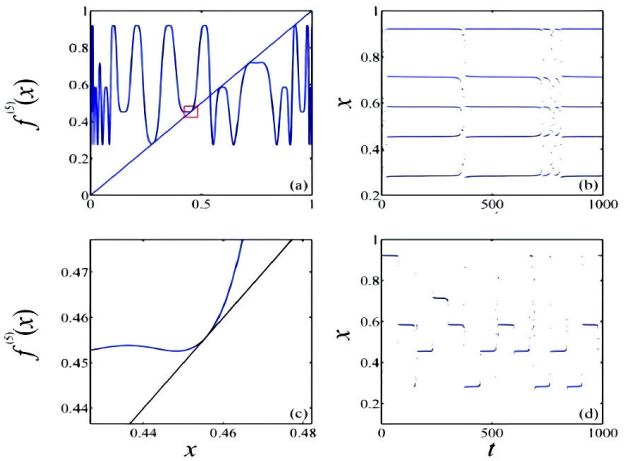

FIGURE 13.Top left panel: Five-times-composed replicator map at the tangent bifurcation of its period five window and a close view below [46]. Top right panel: Trajectory for the conditions in the left panel that imitates the behavioral patterns of a high-dimensional model for ecological evolution.

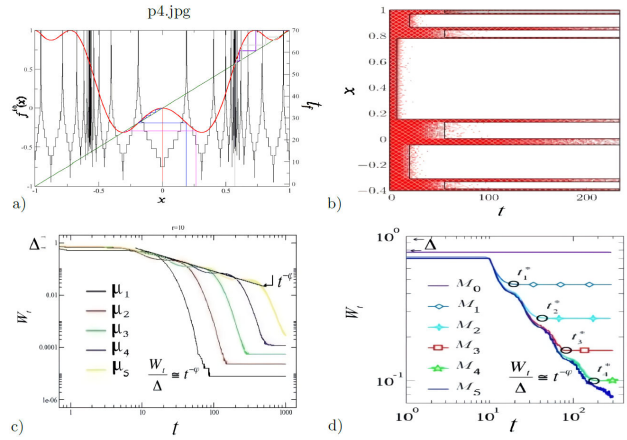

FIGURE 14. a) Flight times t_f (number of iterations) for trajectories to reach the period 4 supercycle attractor. b) Sequential gap formation of an ensemble of trajectories en route to the period-doubling accumulation point attractor, with superimposed sharp transitions approximation (dark line). See text. c) Rate W_t of approach to the supercycle attractors of periods $2^N, N = 1, ..., 5$, in logarithmic scales. See text. d) Same rate W_t for the approach to the Misiurewics points.

quadratic map. The expression descriptive of the population of positions already captured by the attractor resembled that of a partition function. Eventually, this statistical-mechanical likeness became a model for self-organization. Separately, we made use of the trajectory inside the attractor at the period-doubling onset of chaos, which appears as a family of straight lines in logarithmic scales, over several years for distinct purposes, until we realized that it could be obtained analytically from the trajectories of the renormalization-group fixed-point map of another transition to chaos, the tangent bifurcation. Likewise for the quasiperiodic routes to chaos. Therefore all these fixed-point maps share analytic closed forms as well as statistical-mechanical features. Finally, the power law spacing and widths of the windows (that show miniaturized bifurcation diagrams) intertwined along the chaotic-band attractors of the main bifurcation diagram of the quadratic map await their use in the construction of nested models for likewise complex systems.

5.1. Partitions

A decade and a half ago we embarked on a previously (to our knowledge) unreported task. This task consisted of studying ensembles of trajectories evolving towards representative families of attractors of the logistic map. We computed in detail a basic collection of properties that describe those journeys. Firstly, the family of attractors chosen was that of the supercycles together with their accumulation point, the Feigenbaum attractor [47-50]. Lately, we considered the family of Misiurewics points, the attractors at which chaotic bands split [24]. In all cases, we chose ensembles of initial conditions uniformly-distributed across the interval of definition of the map. The properties we monitored were: i) The numbers of iterations necessary for the trajectory initiated at x_0 to reach the attractor (in practice with the necessary use of a small cutoff). We called these times flight-times $t_f(x_0)$ [48,49], see Fig. 14a). ii) The sequential formation of trajectory position gaps in the (x, t) plane [48,50]. See Fig. 14b). And iii) the fraction W_t of phase space $[-1, 1]$ still occupied by the ensemble trajectories at time t [48,50,29], see Figs. 14c) and 14d).

The behavior of the fraction W_t caught our attention. In logarithmic scales (as shown on 14c) and 14d) W_t exhibits the telltale occurrence of discrete scale invariance, power-law decay dressed by logarithmic oscillations, where the latter display the 'recapitulation' property mentioned before, *i.e.* evolution towards 2^n-periodic or 2^n-band chaotic attractors repeats successively the evolution towards those attractors with $2^k, k = 0, 1, 2, ..., n-1$. Sequential band formation and flight-times also show recapitulation. This property implies [48,50] that the fraction W_{2^n} is proportional to the sum of so-called supercycle diameters $d_{n,m}$ [3],

$$W_{2^n} \propto z_n \equiv \sum_{m=0}^{2^{(n-1)}} d_{n,m}, \qquad (30)$$

and likewise for the sum of band widths at the Misiurewics points [24]. We labeled the sum above z_n, as it is sometimes done for partition functions in statistical mechanics, even though it is only a sum of interval lengths. And we began a search for a justification of this impulse.

Only recently [53,54], the first stage in the statistical-mechanical justification of Eq. (30) as a *bona fide* partition function was put together. To begin with, the sequential gap formation in Fig. 14b) was deliberately sharpened so that each family of gaps appears suddenly at fixed given times. This approximation makes this process identical to the con-

struction by stages of a two-scale Cantor set, a multifractal with a partition function

$$z_n = \sum_{l=0}^{n} \binom{n}{l} l_1^{n-l} l_2^{l}, \tag{31}$$

where $l_1 \simeq \alpha^{-1}$ and $l_1 \simeq \alpha^{-2}$, and with α the absolute value of Feigenbaum constant, so that the lengths $L_{n,l} \equiv l_1^{n-l} l_2^{l}, l = 0, 1, 2, ..., n-1$, scale as the diameters and bandwidths do asymptotically in the bifurcation diagram of quadratic maps [53,54]. The next important step was the realization that the same partition function arises in the construction by stages of another kind of multifractal, the two-weight multifractal that consists of progressively subdividing the interval $[0, 1]$, halving the size of compartments successively with weights $W_{n,l} \equiv w_1^{n-l} w_2^{l}, l = 0, 1, 2, ..., n-1$, where $w_1 \simeq \alpha^{-1}$ and $w_2 \simeq \alpha^{-2}$. That is the same Eq. (31) but with l_1 and l_2 replaced by w_1 and w_2 [54]. This partition function is made of compartment or subsystem configurations.

If the initial single compartment contains a thermal system, irrespective of its nature, it finds itself progressively decimated through subdivisions into ever smaller compartments, so that its total conventional entropy gradually diminishes until it finally vanishes. This is the unavoidable effect that self-organization (in our case partitioning) has on the thermal system. But, concurrently, a new statistical-mechanical system develops with its own increasing entropy term as n grows, that related to the partition function z_n above. We found that the dynamics towards the multifractal attractor at the period-doubling onset of chaos is a close analogue to a progressively constrained thermal system [54].

The balance between numbers of configurations and Boltzmann-Gibbs statistical weights of the initial thermal system is strongly altered and ultimately eliminated by the sequential subdivision procedure that mirrors the actions of the attractor. However, the emerging set of subsystem configurations implies a different and novel entropy growth process that eventually upsets the original loss and has the capability of marginally [54] locking the system into a self-organized state with characteristics of criticality, as in the so called self-organized criticality [89]. In the limit $n \to \infty$ self-organization displays the full scale-invariant properties of the transition in or out of chaos, similar to space and time scale invariance of critical states. There, the number of subsystem configurations and their generalized [54] entropy is maximal. As indicated in Ref. [54], attaining this state provides an explanation, within perhaps the simplest model system, for the hypothesis of self-organized criticality [89].

Currently, we are characterizing the sequence of system subdivisions, originally only mirroring the recapitulation property of ensembles of trajectories en route to the attractors, as a sequence of genuine differentiations underlying the bifurcation cascades, of symmetry-breaking phase transitions leading to a marginally stable multi-partitioned state.

5.2. Diagonals

There is a renormalization-group fixed-point map $f^*(x)$ for each limiting stage of the three routes to or out of chaos, period doubling, quasi-periodicity, and intermittency leading to the tangent bifurcation [3-5]. These fixed-point maps embody the universality class property of infinite families of nonlinear dynamical systems. They express the scaling laws stemming from functional composition as the basic feedback element for the transit from regular to chaotic behavior or vice versa. They (arguably) represent the foundation of nonlinear dynamical theory for dissipative systems. Historically, the first case to be worked out was that for period-doubling [3-5], followed by that for quasi-periodicity [3-5], both efforts leading to transcendental functions with no closed-form expressions for $f^*(x)$ [3-5]. The last case obtained was that for the tangent bifurcation [3-5], for which the initially perceived simpler feature of a single attractor-repellor point lead, perhaps not totally unanticipated, to an analytical closed-form expression for $f^*(x)$, as previously shown in Eq. (16) [76]. As recollected here we have relied on these fundamental contributions as the main background support to our studies.

We have made use of fixed-point map $f^*(x)$ trajectories directly or indirectly in all the studies already described. The trajectory at the Feigenbaum point $f_{\mu_\infty}(x)$ initiated at $x_0 = 0$, shown in Fig. 1b), is for all purposes one such case. In Fig. 15a) we show another view for that trajectory, while in Fig. 15b) we show the equivalent result for the golden-mean onset of chaos as obtained from the circle map [11]. On the other hand, we have seen that all the trajectories from the tangent bifurcation fixed-point map in Eq. (16) are given by Eq. (17).

As we have seen, much can be learned by observing the structure of the trajectory positions in 1b) and 15a) as they move in a particularly orchestrated manner across the multifractal attractor. In logarithmic scales the trajectory separates into equally-spaced horizontal bands, with half of the positions in the top band (odd iteration times in Fig. 1b) and even iteration times in 15a). Subsequent horizontal bands contain $2^{-n}, n = 2, 3, ...$, fractions of the remaining positions. Each band consists of sub-bands, and so on. The band structure expresses geometrically the scaling features of the functional composition $f^*(x)$. As shown in Fig. 15b) there is a similar band structure for the golden-mean trajectory but it is more difficult to explore it only by means of logarithmic scales.

But the main feature of these trajectories we focus on here are the 'diagonals' we described much earlier. See the text below Eq. (1). The entire trajectory $x_t = f_{\mu_\infty}^{(t)}(x_0 = 0)$ can be decomposed into position sub-sequences all of which obey the same power-law decay. Also, we saw that such diagonals possess the ideal glass perfect aging scaling property. See the text around Eq. (8). The alternate view of this trajectory shown in Fig. 15b), as well as that for the golden-mean in Fig. 15b) can be also decomposed into 'diagonals', and these diagonals can be expressed analytically as q-deformed expo-

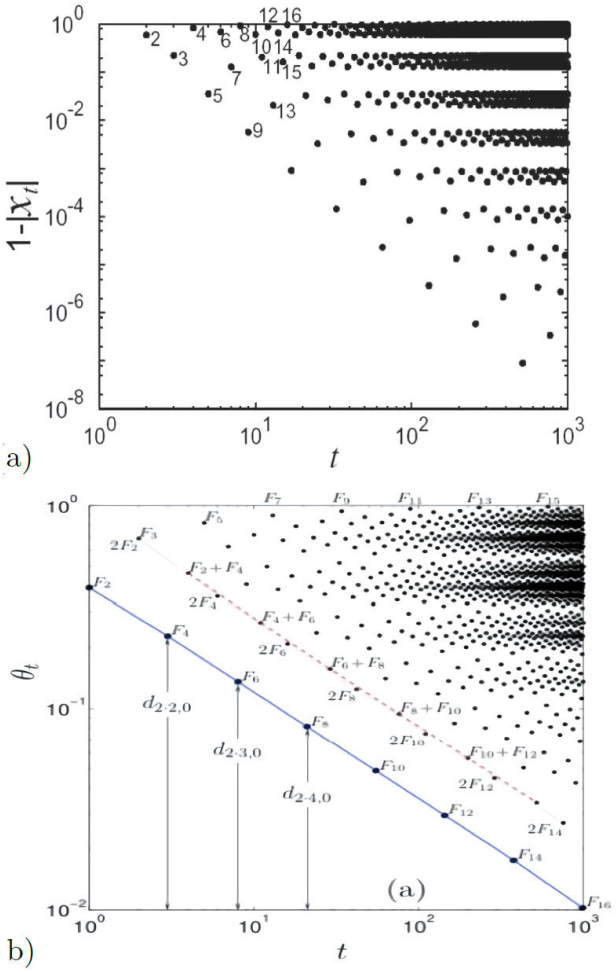

FIGURE 15. a) Distance from $x = 1$ of the absolute values of positions in logarithmic scales of the first 1000 iterations for the trajectory at the period-doubling onset of chaos for the logistic map. The numbers correspond to iteration times. See Fig. 1b). b) Positions in logarithmic scales of the first 1000 iterations for the trajectory at the golden mean onset of chaos for the circle map. The F_n are Fibonacci numbers in the position labels that correspond to iteration times. In both cases a) and b) the power-law decay of positions along the time sub-sequences described in the text can be clearly appreciated.

nentials, *e.g.* Eq. (8). See also Ref. [30] for other cases, including the first diagonal of the golden-mean trajectory.

The recent idea or question that has made us revisit the trajectory features we call diagonals is the realization that all the fixed-point maps $f^*(x)$, for the three routes, are more closely related than originally thought, and that they share, amongst other ingredients, the same closed-form analytic expression that was first found for the tangent bifurcation [to be published]. Our intention was to find an alternative way to obtain the multifractal trajectories produced by the known fixed-point maps $f^*(x)$ for period doubling and quasi-periodicity. That is, the program we followed was to reproduce the master trajectories $f^{*(t)}(x_0)$ in 15a), and 15b), diagonal by diagonal, from the tangent bifurcation trajectories $f^{*(t)}(x_0)$

$$x_t = f^{*(t)}(x_0) = x_0 \exp_z(|x_0|^{z-1} u t). \qquad (32)$$

Each diagonal, say, $D_k, k = 1, 2, ...$, requires one initial condition $x_0^{(k)}$ and an iteration time transformation from the consecutive times in Eq. (32) to the diagonal sub-sequence times, say, $\tau^{(k)}$. Each route to chaos fixes the value of the deformed exponential parameter z as well as that for the curvature parameter u [to be published].

This hitherto unseen connection between all the classical transitions to chaos constitutes a formal advance about the required mathematical structure of viable fixed points maps $f^*(x)$, those that express the universal scaling features of general families or classes of nonlinear dynamical systems when driven into regime borderlines. But also, as we have seen, to the occurrence of q-generalized entropies in the statistical-mechanical descriptions mentioned here. This applies to our model perspectives for glass formation, critical fluctuations and localization transitions in condensed matter physics, more generally, to complex systems paradigms and self-organization, and also to our simplified modeling and treatments to diversity, ranked data, networks from time series, correlated random walks, and certain specific game-theoretical situations.

5.3. Windows

There is a collection of features in the classic bifurcation diagram for quadratic maps that have been left out so far in our discussions. These features are related to the infinite collection of interruptions, called 'windows', of the chaotic band attractors sets displayed along $\mu > \mu_\infty$, and shown in Fig. 16a). There is an infinite number of windows that contain families of reproductions of the bifurcation diagram itself, and again, repeatedly, within each smaller replica, since the bifurcation diagram is a fractal object. The interruptions display power-law spacing and widths that have been characterized a long time ago [55,56]. The same window features occur across the bifurcation diagrams of many other low-dimensional iterated maps, including those for the circle maps [3-5] with two control parameters, and also that other two-parameter bifurcation diagram we mentioned briefly for the replicator map in Eq. (29).

There are other related structures in the quadratic map bifurcation diagram that are worth mentioning here. These are the so-called 'shadow' curves and their dual 'period' curves [90]. The first set is given by the set of functions $x(\mu) = f_\mu^{(2^n)}(0), n = 0, 1, ...$, while the second set by the solutions of $x = f_\mu^{(2^n)}(x), n = 0, 1, ...$, both as a function of μ. See 16b) and 16c). The shadow curves have mutual points of tangency and also intersect themselves at the Misiurewics points, they envelop the bifurcation replicas within the windows. The period curves trace the periodic solutions independently of whether they are stable (attractors) or unstable (repellors). The two sets of shadow and periodic curves

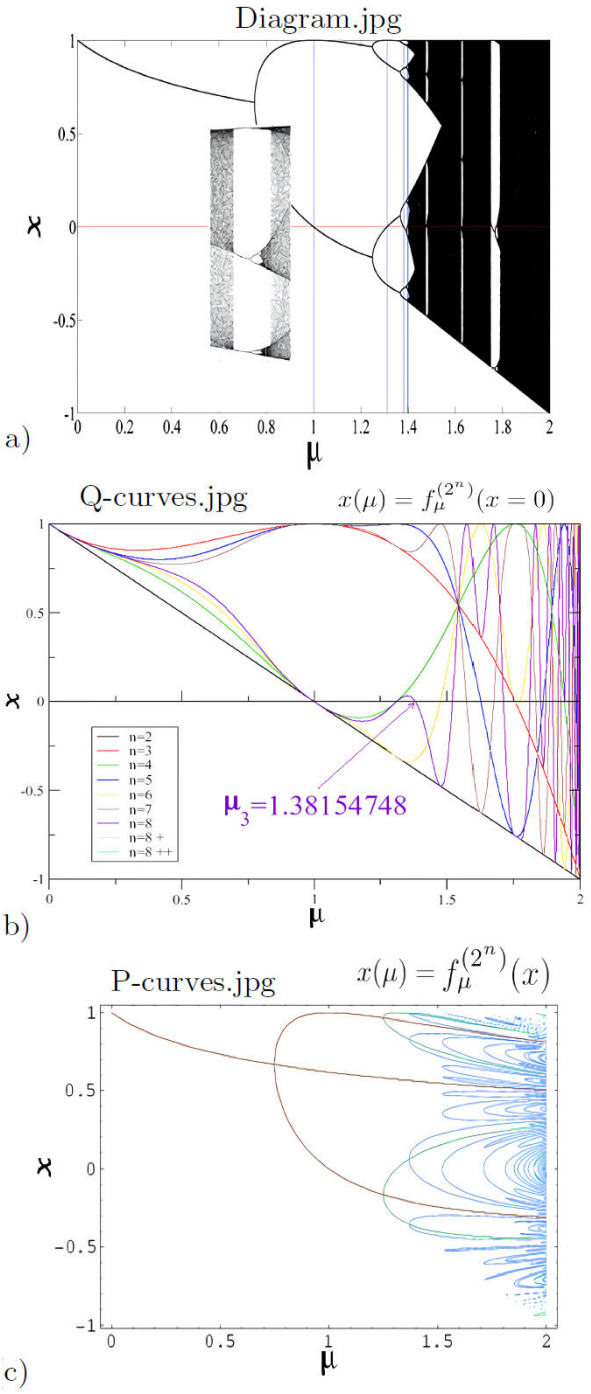

FIGURE 16. a) Widely-known logistic map bifurcation diagram showing strip windows in the chaotic regime and an amplification of the widest (period three) window. b) Shade curves outlining the bifurcation diagram in a) See text. c) Period curves where both stable and unstable periodic solutions are shown. See text.

interact, they are tangent at the pitchfork bifurcations within the windows.

We had already made use of the windows in the bifurcation diagram, but only marginally, by using the properties in the chaotic neighborhood of their tangent bifurcation borders, the existence of the infinite set of windows was used to construct a simple model [45,46] to reproduce the punctuated equilibrium [86] observed in the nature of evolutionary ecology, that is captured by Jensen's TaNa model [86]. But other insights are awaiting for the more complete use of the features of the sets of windows, for example, for the construction of simple enough models that would describe complex systems where the most significant property is embedding, nested systems within systems. Like the case of the microbiota, the ecological communities of microorganisms found in and on all multicellular organisms from plants to animals [91].

The different sets of power laws displayed by the families of windows make certain the existence of generalized statistical-mechanical behaviors not yet characterized, as other sets of power laws occurring in the dynamics of quadratic and related maps have been, *e.g.* as in all the previous subsections. These, say still 'idle', sets of power laws correspond to the spacing of the windows across the bifurcation diagram, their widths, and other features within them, as are the replicas of the main cascades in the primary diagram. Additionally, this complex structure is wrapped by the intricate system of shadow and period curves.

6. Outlook

As future directions, we put together a list of idealizations or models, unpretentious but effective for providing specific answers to complex systems problems and subjects. Currently, they are at different stages of development, and all are based on the nonlinear dynamical content in each of our twelve sets of studies:

Sensitivities. A model for the ideal growth of diversity, a mainstay 'phylogenetic tree', based on the period doubling route to chaos, and its recapitulation at the transition to chaos. In its base format diversity is quantified via the anomalous, multifractal, sensitivity to initial conditions.

Glasses. A model for the flow (and arrest) of traffic (animal, human, vehicular) that makes use of our discovery of the manifestation of vitreous dynamics in the noise-induced bifurcation gap at the onset of chaos.

Localizations. A model for collective behavior in complex systems based on coherent communication states resembling those described here for wave propagation through scattering media.

Sums. A model of correlated walks that displays progressively anomalous diffusion and arrest based on sums of position trajectories across the chaotic-band attractors of quadratic maps.

Rankings. A model for ranked distributions based on nonlinear dynamics near or at tangent bifurcations that reveals universality classes and borderline dimensionality (as in critical phenomena), with links to number theory (in particular prime numbers for the class that corresponds to the empirical Zipf law).

Fluctuations. A model for the identification of early warnings based on our studies on the spatial structure and

temporal evolution of the dominant fluctuations at a critical point.

Networks. A model statistical-mechanical structure for a class of networks, those obtained via the HV algorithm from time series formed by trajectories along the period doubling and all the quasi-periodic routes to chaos.

Measures. A model to observe the equivalence between the two main paradigms for the understanding of complex systems in recent decades: edge of chaos and criticality.

Games. A phenomenological model based on sequences of transitions to chaos via intermittency that reproduces quasi-stable states descriptive of punctuated equilibrium observed in the evolution of ecosystems (biological, urban, technological).

Partitions. A model capable of offering a physical basis to self-organization, analogous to the non-linear dynamics towards the attractors that form the period-doubling and chaotic-band splitting cascades in quadratic maps.

Diagonals. A pathway to demonstrate the general occurrence of q-generalized statistical-mechanical properties in all the models of this list provided by the recently realized link between all renormalization-group fixed-point maps at the transitions to chaos.

Windows. Models constructed to describe complex systems where the most significant property is embedding, systems nested within systems.

The twelve units of studies we described are interrelated in various ways. To highlight these, as in a zodiac, they could have been grouped differently, into four classes that underline another common traits, or distributed in three groups containing each four studies that share the same quality, or separated into only two sets of six studies each (or vice versa), to classify them according to other common characteristic, and so on. Connections amongst these dozen research lines become evident with each of these different allocations. We chose a classification that reflects only circumstances in their elaboration.

Acknowledgements

AR is profoundly thankful to all his collaborators over the years and deeply appreciative to all colleagues with whom valuable discussions took place. Support is acknowledged from IN106120-PAPIIT-DGAPA-UNAM.

1. Alberto Robledo, Generalized statistical mechanics at the onset of chaos. *Entropy* **15** (2013) 5178. https://doi.org/10.3390/e15125178
2. C. Velarde and A. Robledo. Manifestations of the onset of chaos in condensed matter and complex systems. *Eur. Phys. J. Spec. Top.* **227** (2018) 645. https://doi.org/10.1140/epjst/e2018-00128-9
3. H.G. Schuster, *Deterministic chaos. An Introduction*. 2nd Ed. (VCH Publishers, Weinheim, Germany, 1988).
4. C. Beck and F. Schlogl, *Thermodynamics of Chaotic Systems*. (Cambridge, University Press, Cambridge, UK, 1993).
5. R.C. Hilborn. *Chaos and Nonlinear Dynamics*. 2nd Ed. (Oxford University Press, New York, NY, USA, 2000).
6. F. Baldovin and A. Robledo, Sensitivity to initial conditions at bifurcations in one-dimensional nonlinear maps: Rigorous nonextensive solutions". *EPL* **60** (2002) 518. https://doi.org/10.1209/epl/i2002-00249-7
7. F. Baldovin and A. Robledo, Universal renormalization-group dynamics at the onset of chaos in logistic maps and nonextensive statistical mechanics. *Phys. Rev. E* **66** (2002) 045104. https://www.doi.org/10.1103/PhysRevE.66.045104
8. A. Robledo, Criticality in nonlinear one-dimensional maps: RG universal map and nonextensive entropy. *Physica D* **193** (2004) 153-160. https://doi.org/10.1016/j.physd.2004.01.016
9. F. Baldovin and A. Robledo, Nonextensive Pesin identity: Exact renormalization group analytical results for the dynamics at the edge of chaos of the logistic map. *Phys. Rev. E* **69** (2004) 045202. https://www.doi.org/10.1103/PhysRevE.69.045202
10. E. Mayoral and A. Robledo. Tsallis q index and Morils q phase transitions at the edge of chaos. *Phys. Rev. E* **72** (2005) 026209. https://www.doi.org/10.1103/PhysRevE.72.026209
11. H. Hernandez-Saldaña and A. Robledo, Dynamics at the quasiperiodic onset of chaos, Tsallis q-statistics and Mori's q-phase thermodynamics. *Physica A* **370** (2006) 286. https://doi.org/10.1016/j.physa.2006.03.018
12. A. Robledo, Incidence of nonextensive thermodynamics in temporal scaling at Feigenbaum points. *Physica A* **370** (2006) 449. https://doi.org/10.1016/j.physa.2006.06.003
13. A. Robledo, Universal glassy dynamics at noise-perturbed onset of chaos: a route to ergodicity breakdown. *Phys. Lett. A* **328** (2004) 467. https://doi.org/10.1016/j.physleta.2004.06.062
14. A. Robledo, Aging at the edge of chaos: Glassy dynamics and nonextensive statistics". *Physica A* **342** (2004) 104. https://doi.org/10.1016/j.physa.2004.04.065
15. F. Baldovin and A. Robledo, Glassy dynamics at the onset of chaos with additive noise. *Fluctuation and Noise Letters* **5** (2005) L313. https://doi.org/10.1142/S0219477505002707
16. F. Baldovin and A. Robledo, Parallels between the dynamics at the noise-perturbed onset of chaos in logistic maps and the dynamics of glass formation. *Phys. Rev. E* **72** (2005) 066213. https://www.doi.org/10.1103/PhysRevE.72.066213

17. M. Martínez-Mares and A. Robledo, Equivalence between the mobility edge of electronic transport on disorderless networks and the onset of chaos via intermittency in deterministic maps. *Phys. Rev. E* **80** (2009) 045201. https://www.doi.org/10.1103/PhysRevE.80.045201

18. Y. Jiang *et al.* , Möbius transformations and electronic transport properties of large disorderless networks, *Phys. Rev. E* **85** (2012) 057202. https://doi.org/10.1103/PhysRevE.85.057202

19. M. Martínez-Mares, V. Domínguez-Rocha, and A. Robledo, Typical length scales in conducting disorderless networks. *Eu. Phys. J. Spec. Top.* **226** (2017) 417. https://doi.org/10.1140/epjst/e2016-60129-x

20. V. Domínguez-Rocha *et al*., Invariant density of intermittent nonlinear maps descriptive of coherent quantum transport through disorderless lattices. *Physica D* **412** (2020) 132623, https://doi.org/10.1016/j.physd.2020.132623

21. M. A. Fuentes and A. Robledo, Renormalization group structure for sums of variables generated by incipiently chaotic maps. *J. Statis. Mech. Theory Exp.* **2010** (2010) P01001. https://doi.org/10.1088/1742-5468/2010/01/P01001

22. M. A. Fuentes and A. Robledo, Stationary distributions of sums of marginally chaotic variables as renormalization group fixed points. *J. Phys.: Conf. Ser*. **201** (2010) 012002. https://doi.org/10.1088/1742-6596/201/1/012002

23. M. A. Fuentes and A. Robledo, Sums of variables at the onset of chaos. *Eur. Phys. J. B* **87** (2014) 32. https://doi.org/10.1140/epjb/e2014-40882-1

24. A. Díaz-Ruelas, M. Angel Fuentes, and A. Robledo, Scaling of distributions of sums of positions for chaotic dynamics at band-splitting points. *EPL* **108** (2014) 20008. https://doi.org/10.1209/0295-5075/108/20008

25. A. Diaz-Ruelas and A. Robledo, Sums of variables at the onset of chaos, replenished. *Eur. Phys. J. Special Topics* **225** (2016) 2763, https://doi.org/10.1140/epjst/e2016-60011-y

26. C. Altamirano and A. Robledo, Generalized thermodynamics underlying the laws of Zipf and Benford. *International Conference on Complex Sciences. Springer*. (2009) 2232. https://doi.org/10.1007/978-3-642-02469-6_100

27. C. Altamirano and A. Robledo, Possible thermodynamic structure underlying the laws of Zipf and Benford. *Eur. Phys. J. B* **81** (2011) 345. https://doi.org/10.1140/epjb/e2011-10968-5

28. A. Robledo, Laws of Zipf and Benford, intermittency, and critical fluctuations. *Chin. Sci.Bull.* **56** (2011) 3643, https://doi.org/10.1007/s11434-011-4827-y

29. G. Cigdem Yalcin, A. Robledo, and M. Gell-Mann, Incidence of q-statistics in rank distributions. *PNAS* **111** (2014) 14082. https://doi.org/10.1073/pnas.1412093111

30. G. Cigdem Yalcin, C. Velarde, and A. Robledo. Entropies for severely contracted configuration space. *Heliyon* **1** (2015) e00045. https://doi.org/10.1016/j.heliyon.2015.e00045

31. C. Velarde and A. Robledo. Rank distributions: Frequency vs. magnitude. *PLOS One* **12** (2017) e0186015. Ed. by Miguel A. F. Editor Sanjun, http://dx.doi.org/10.1371/journal.pone.0186015

32. C. Velarde and A. Robledo, Dynamical analogues of rank distributions. *PLOS One* **14** (2019) 1. https://doi.org/10.1371/journal.pone.0211226

33. A Robledo. Unorthodox properties of critical clusters. *Mol. Phys.* **103** (2005) 3025. https://doi.org/10.1080/00268970500185989

34. A. Robledo, q-statistical properties of large critical clusters. *Int. J. Mod. Phys. B* **21** (2007) 3947. https://doi.org/10.1142/S0217979207045001

35. M. Riquelme-Galván and A. Robledo, Dual characterization of critical fluctuations: Density functional theory and nonlinear dynamics close to a tangent bifurcation. *Eur. Phys. J. Special Topics* **226** (2017) 433. https://doi.org/10.1140/epjst/e2016-60268-0

36. B. Luque *et al*., Feigenbaum graphs: a complex network perspective of chaos. *PLoS One* **6** (2011) e22411. https://doi.org/10.1371/journal.pone.0022411

37. B. Luque *et al*. Analytical properties of horizontal visibility graphs in the Feigenbaum scenario. *Chaos* **22** (2012) 013109. https://doi.org/10.1063/1.3676686

38. B. Luque, L. Lacasa, and A. Robledo, Feigenbaum graphs at the onset of chaos. *Phys. Lett. A* **376** (2012) 3625. https://doi.org/10.1016/j.physleta.2012.10.050

39. B. Luque *et al.*, Quasiperiodic graphs: Structural design, scaling and entropic properties. *J. Nonlinear Sci.* **23** (2013) 335. https://doi.org/10.1007/s00332-012-9153-2

40. A. M. Nú nez *et al.*, Horizontal visibility graphs generated by type-I intermittency. *Phys. Rev. E* **87** (2013) 052801. https://www.doi.org/10.1103/PhysRevE.87.052801

41. B. Luque *et al.*, Quasiperiodic graphs at the onset of chaos. *Phys. Rev. E* **88** (2013) 062918. https://www.doi.org/10.1103/PhysRevE.88.062918

42. B. Luque *et al.*, Entropy and renormalization in chaotic visibility graphs. *Mathematical Foundations and Applications of Graph Entropy*. Wiley Online Library, **6** (2017) 1. https://doi.org/10.1002/9783527693245.ch1

43. F. Baldovin, A. Diaz-Ruelas, and A. Robledo, Entropy of trajectories along period doubling and chaotic-band splitting cascades, *Chaos J. Nonlinear Sci.* (2020, in preparation).

44. D. Vilone, A. Robledo, and A. Sánchez. Chaos and unpredictability in evolutionary dynamics in discrete time. *Phys. Rev. Lett.* **107** (2011) 038101. https://doi.org/10.1103/PhysRevLett.107.038101

45. A. Diaz-Ruelas *et al*., Tangent map intermittency as an approximate analysis of intermittency in a high dimensional fully stochastic dynamical system: The Tangled Nature model. *Chaos* **26** (2016) 123105. https://doi.org/10.1063/1.4968207

46. A. Diaz-Ruelas *et al*., Relating high dimensional stochastic complex systems to low-dimensional intermittency. *Eur. Phys. J. Spec. Top.* **226** (2017) 341. issn: 1951-6401. http://dx.doi.org/10.1140/epjst/e2016-60264-4

47. A. Robledo and L.G. Moyano, Some aspects of the dynamics towards the supercycle attractors and their accumulation point, the Feigenbaum attractor. *AIP Conference Proceedings*. **965** (2007) 114. https://doi.org/10.1063/1.2828722

48. A. Robledo and L. G. Moyano. q-deformed statistical-mechanical property in the dynamics of trajectories en route to the Feigenbaum attractor. *Phys. Rev. E* **77** (2008) 036213. https://doi.org/10.1103/PhysRevE.77.036213

49. L. G. Moyano, D. Silva, and A. Robledo, Labyrinthine pathways towards supercycle attractors in unimodal maps. *Central Eur. J. Phys.* **7** (2009) 591. https://doi.org/10.2478/s11534-009-0065-1

50. A. Robledo and L.G. Moyano, Dynamics towards the Feigenbaum attractor. *Braz. J. Phys.* **39** (2009) 364. https://doi.org/10.1590/S0103-97332009000400004.

51. A. Robledo, q-deformed statistical-mechanical structure in the dynamics of the Feigenbaum attractor". *J. Phys. Conf. Ser.* **246** (2010) 012025. https://doi.org/10.1088/1742-6596/246/1/012025

52. A. Robledo, A dynamical model for hierarchy and modular organization: The trajectories en route to the attractor at the transition to chaos. *J. Phys. Conf. Ser.* **394** (2012) 012007. https://doi.org/10.1088/1742-6596/394/1/012007

53. A. Diaz-Ruelas and A. Robledo, Emergent statistical-mechanical structure in the dynamics along the period-doubling route to chaos. *EPL* **105** (2014) 40004. https://doi.org/10.1209/0295-5075/105/40004

54. A. Robledo, Self-organization and a constrained thermal system analogue of the onset of chaos. *EPL* **123** (2018) 40003. https://doi.org/10.1209%2F0295-5075%2F123%2F40003.

55. J. A. Yorke *et al.*, Scaling Behavior of Windows in Dissipative Dynamical Systems. *Phys. Rev. Lett.* **54** (1985) 1095. https://doi.org/10.1103/PhysRevLett.54.1095

56. H.W. Capel and J. P. van der Weele. Window scaling in one-dimensional maps. Physics Letters A **136** (1990) 109.

57. V. Latora, A. Rapisarda, and A. Robledo, Revisiting disorder and Tsallis statistics. *Science* **300** (2003) 250. https://doi.org/10.1126/science.300.5617.249d

58. A. Robledo, Unifying laws in multidisciplinary power-law phenomena: fixed-point universality and nonextensive entropy. *Nonextensive Entropy Interdisciplinary Applications*. (Oxford University Press, 2004), pp. 63.

59. A. Robledo, Intermittency at critical transitions and aging dynamics at the onset of chaos. *Pramana* **64** (2005) 947. https://www.ias.ac.in/article/fulltext/pram/064/06/0947-0956

60. A. Robledo, Critical attractors and q-statistics. *Europhysics News* **36** (2005) 214. https://doi.org/10.1051/epn:2005611

61. A. Robledo, F. Baldovin, and E. Mayoral, Two stories outside Boltzmann-Gibbs statistics: Mori q-phase transitions and glassy dynamics at the inset of chaos. *Complexity, Metastability and Nonextensivity. World Scientific*, (2005) 43. https://doi.org/10.1142/9789812701558_0004

62. E Mayoral and A Robledo. A recent appreciation of the singular dynamics at the edge of chaos. The Logistic Map and the Route to Chaos. Springer, (2006) pp. 339-354.

63. A. Robledo, Crossover from critical to chaotic attractor dynamics in logistic and circle maps. *Prog. Theor. Phys. Supp.* **162** (2006) 10. https://doi.org/10.1143/PTPS.162.10

64. A. Robledo, Critical Attractors and the Physical Realm of qs-tatistics. *Chaos, Nonlinearity, Complexity*. (Springer, Berlin, 2006). pp. 72-113.

65. A. Robledo, *Gensis de una nueva fisica estadistica. Descubrimientos y Aportaciones Cientificas y Humanisticas Mexicanas en el Siglo Veinte*, (Academia Mexicana de Ciencias; Fondo de Cultura Economica, 2006).

66. C. Velarde and A. Robledo, Pascal (Yang Hui) triangles and power laws in the logistic map. *J. Phys. Conf. Ser.* **604** (2015) 012018. https://doi.org/10.1088/1742-6596/604/1/012018

67. M.O. Hill, Diversity and Evenness: A Unifying Notation and Its Consequences. *Ecology* **54** (1973) 427. https://doi.org/10.2307/1934352

68. T. Li, Nonlinear dynamics of traffic jams. *Physica D* **207** (2005) 41. https://doi.org/10.1016/j.physd.2005.05.011

69. A.S. de Wijn *et al*., Criticality in dynamic arrest: Correspondence between glasses and traffic. *Phys. Rev. Lett.* **109** (2012) 228001. https://doi.org/10.1103/PhysRevLett.109.228001

70. X.-J. Wang P. Gaspard, Sporadicity: Between periodic and chaotic dynamical behaviors. *PNAS* **85** (1988) 4591. https://dx.doi.org/10.1073%2Fpnas.85.13.4591

71. S. A. Marvel, R. E. Mirollo, and S. H. Strogatz, Identical phase oscillators with global sinusoidal coupling evolve by M´obius group action. *Chaos* **19** (2009) 043104. https://doi.org/10.1063/1.3247089

72. M. C. Mackey and M. Tyran-Kamiska, Deterministic Brownian motion: The effects of perturbing a dynamical system by a chaotic semi-dynamical system. *Phys. Rep.* **422** (2006) 167. https://doi.org/10.1016/j.physrep.2005.09.002

73. U. Tirnakli, Christian Beck, and C. Tsallis, Central limit behavior of deterministic dynamical systems. *Phys. Rev. E* **75** (2007) 040106(R). https://doi.org/10.1103/PhysRevE.75.040106

74. Ugur Tirnakli, Constantino Tsallis, and Christian Beck. Closer Look at Time Averages of the Logistic Map at the Edge of Chaos. *Phys. Rev. E* **79** (2009) 056209. https://doi.org/10.1103/PhysRevE.79.056209

75. L. Pietronero *et al.*, The uneven distribution of numbers in nature. *Physica A* **293** (2001) 297. https://doi.org/10.1016/S0378-4371(00)00633-6

76. B. Hu and J. Rudnick, Exact solutions to the Feigenbaum renormalizationgroup equations for intermittency. *Phys. Rev. Lett.* **48** (1982) 1645. 1645. https://doi.org/10.1103/PhysRevLett.48.1645

77. N. G. Antoniou *et al.*, Fractals at T = Tc due to Instanton-like Configurations. *Phys. Rev. Lett.* **81** (1998) 4289. https://doi.org/10.1103/PhysRevLett.81.4289

78. Y.F. Contoyiannis and F.K. Diakonos, Criticality and intermittency in the order parameter space. *Phys. Lett. A* **268** (2000) 286. https://doi.org/10.1016/S0375-9601(00)00180-8

79. L. Lacasa *et al.*, From time series to complex networks: the visibility graph.*PNAS* **105** (2008) 4972. https://doi.org/10.1073/pnas.0709247105

80. A. Robledo, Renormalization group, entropy optimization, and nonextensivity at criticality. *Phys. Rev. Lett.* **83** (1999) 2289. https://doi.org/10.1103/PhysRevLett.83.2289

81. N.G. van Kampen. *Stochastic Processes in Physics and Chemistry*. 3rd ed. (Elsevier, BV, North Holland, 2007).

82. P. Cvitanovic. Chaos: Classical and Quantum. Santa Fe, USA: Complexity Explorer, Santa Fe Institute, 2015. https://www.complexityexplorer.org/explore/resources/612-chaos-book

83. P. Gaspard. *Chaos,scattering and statistical mechanics*. (Cambridge University Press, Cambridge, UK, 1998).

84. M.A. Nowak. *Evolutionary Dynamics: Exploring the Equations of Life*. (Harvard University Press, Cambridge, MA, USA, 2006).

85. D. Piovani, J. Grujic, and H.J. Jensen, Linear stability theory as an early warning sign for transitions in high dimensional complex systems. *J. Phys. A: Math. Theor.* **49** (2016) 295102. https://doi.org/10.1088/1751-8113/49/29/295102

86. K. Christensen *et al.*, Tangled nature model: A model of evolutionary ecology. *J. Theo. Bio.* **216** (2002) 2289. https://doi.org/10.1006/jtbi.2002.2530

87. G.U. Yule, A Mathematical Theory of Evolution. *Philos. Trans. R. Soc. Lond., B, Biol. Sci.*. **213** (1925) 21. https://doi.org/10.1098/rstb.1925.0002

88. A.-L. Barabasi and R. Albert. Emergence of scaling in random networks". *Science* **286** (1999), pp. 509-512.

89. H.J. Jensen. *Self-organized Criticality*. (Cambridge University Press, Cambridge, UK, 1998).

90. C. Ross, M. Odell, and S. Cremer, The shadow-curves of the orbit diagram permeate the bifurcation diagram, too. *Int. J. Bifurcat. Chaos* **19** (2009) 3017. https://doi.org/10.1142/S0218127409024621

91. E. Rosenberg and I. Zilber-Rosenberg. The Hologenome Concept: Human, *Animal and Plant Microbiota*. Switzerland: (Springer International Publishing, Switzerland, 2013).